DEVELOPMENT

Site-specific methylation of Notch1 controls the amplitude and duration of the Notch1 response

Kerstin Hein,[1,2] Gerhard Mittler,[1,3] Wiebke Cizelsky,[4] Michael Kühl,[4] Francesca Ferrante,[2] Robert Liefke,[5] Ina M. Berger,[6] Steffen Just,[6] J. Eric Sträng,[7] Hans A. Kestler,[7,8] Franz Oswald,[9]* Tilman Borggrefe[1,2]*

Physiologically, Notch signal transduction plays a pivotal role in differentiation; pathologically, Notch signaling contributes to the development of cancer. Transcriptional activation of Notch target genes involves cleavage of the Notch receptor in response to ligand binding, production of the Notch intracellular domain (NICD), and NICD migration into the nucleus and assembly of a coactivator complex. Posttranslational modifications of the NICD are important for its transcriptional activity and protein turnover. Deregulation of Notch signaling and stabilizing mutations of Notch1 have been linked to leukemia development. We found that the methyltransferase CARM1 (coactivator-associated arginine methyltransferase 1; also known as PRMT4) methylated NICD at five conserved arginine residues within the C-terminal transactivation domain. CARM1 physically and functionally interacted with the NICD-coactivator complex and was found at gene enhancers in a Notch-dependent manner. Although a methylation-defective NICD mutant was biochemically more stable, this mutant was biologically less active as measured with Notch assays in embryos of *Xenopus laevis* and *Danio rerio*. Mathematical modeling indicated that full but short and transient Notch signaling required methylation of NICD.

INTRODUCTION

Notch signaling regulates various processes during development. However, aberrant Notch signaling—through *NOTCH1* mutations or dysregulation—contributes to human disease, such as cancer. Notch signal transduction is mediated by a highly conserved signaling pathway that is activated upon cell-to-cell contact (*1*). Ligand binding induces specific proteolytic cleavage events within the Notch receptor, resulting in a γ-secretase–dependent release of the Notch intracellular domain (NICD). NICD migrates into the nucleus, binds to the basal transcription factor RBP-J, also known as CSL [CBF1, Su(H), Lag-1], and activates transcription of target genes. The timing of the Notch response is tightly regulated by receptor-ligand interaction, proteolytic processing, and turnover of the NICD (*2*, *3*). Posttranslational modifications such as phosphorylation (*4*–*6*), acetylation (*7*), and ubiquitination (*8*) determine the protein half-life of NICD. So far, ubiquitination has been best described: the E3 ubiquitin ligase FBXW7 (also known as SEL10 or CDC4), first discovered to play a role in Notch signaling in *Caenorhabditis elegans* (*9*), ubiquitinates the nuclear form of the activated Notch receptor (*10*), thereby marking NICD for its rapid degradation by the proteasome. In leukemia cells, *FBXW7* mutations stabilize NICD, leading to Notch pathway dysregulation (*11*, *12*). Thus, mutations not only in Notch1 itself but also in Notch modifiers contribute to the pathology of cancer (*13*, *14*).

Protein arginine methyltransferases (PRMTs) have been described in many species. They can methylate the terminal guanidino groups either asymmetrically [asymmetric dimethylated arginine (aDMA)] or symmetrically [symmetric dimethylated arginine (sDMA)]. Thereby, they are classified as type I (aDMA) or type II (sDMA) PRMTs [reviewed in (*15*)]. Arginine methylation emerges as a crucial regulatory mechanism in a variety of important cellular functions, for example, signaling (*16*, *17*) and gene regulation (*18*–*20*). The type I methyltransferase CARM1 (coactivator-associated arginine methyltransferase 1; also known as PRMT4) was first identified as coactivator of steroid receptor signaling (*21*, *22*). Knockout of CARM1 confirmed the essential unique function of the methyltransferase that cannot be compensated by other PRMTs. CARM1 knockout mice die just after birth and are smaller than their littermates (*23*). The enzymatic activity of CARM1 is required for all of its known in vivo functions (*24*). Here, we investigated whether the NICD itself is targeted by the chromatin modifier CARM1 and subsequently characterized the functional role of CARM1-dependent Notch methylation in the stability and activity of the NICD in vivo.

RESULTS

The C-terminal part of the NICD is methylated by CARM1

To investigate whether NICD itself is methylated at arginine residues, we performed Western blotting using two commercial antibodies recognizing either asymmetrically methylated arginine (ASYM24) or symmetrically methylated arginine (SYM11). Bovine serum albumin (BSA) coupled to aDMA or sDMA was used as a positive control. The NICD, which was affinity-purified using a biotinylation tagging system as previously described (*25*), was recognized by the ASYM24 antibody but not by the SYM11 antibody (Fig. 1A and fig. S1A), suggesting that the arginine(s) in NICD is asymmetrically dimethylated. The main part of asymmetric arginine dimethylation is mediated by the type I arginine methyltransferase PRMT1,

[1]Max-Planck-Institute of Immunobiology and Epigenetics, 79108 Freiburg, Germany. [2]Institute of Biochemistry, University of Giessen, 35392 Giessen, Germany. [3]BIOSS, Center for Biological Signalling Studies, University of Freiburg, Schänzlestrasse 18, 79104 Freiburg, Germany. [4]Institute for Biochemistry and Molecular Biology, Ulm University, 89081 Ulm, Germany. [5]Department of Cell Biology, Harvard Medical School and Division of Newborn Medicine, Boston Children's Hospital, Boston, MA 02215, USA. [6]Department of Internal Medicine II, Center for Internal Medicine, University Medical Center Ulm, 89081 Ulm, Germany. [7]Core Unit Medical Systems Biology, Institute of Neural Information Processing, Ulm University, 89069 Ulm, Germany. [8]Friedrich-Schiller University and Fritz Lipmann Institute, Leibniz Institute for Aging Research, D-07745 Jena, Germany. [9]Department of Internal Medicine I, Center for Internal Medicine, University Medical Center Ulm, 89081 Ulm, Germany.
*Corresponding author. E-mail: tilman.borggrefe@biochemie.med.uni-giessen.de (T.B.); franz.oswald@uni-ulm.de (F.O.)

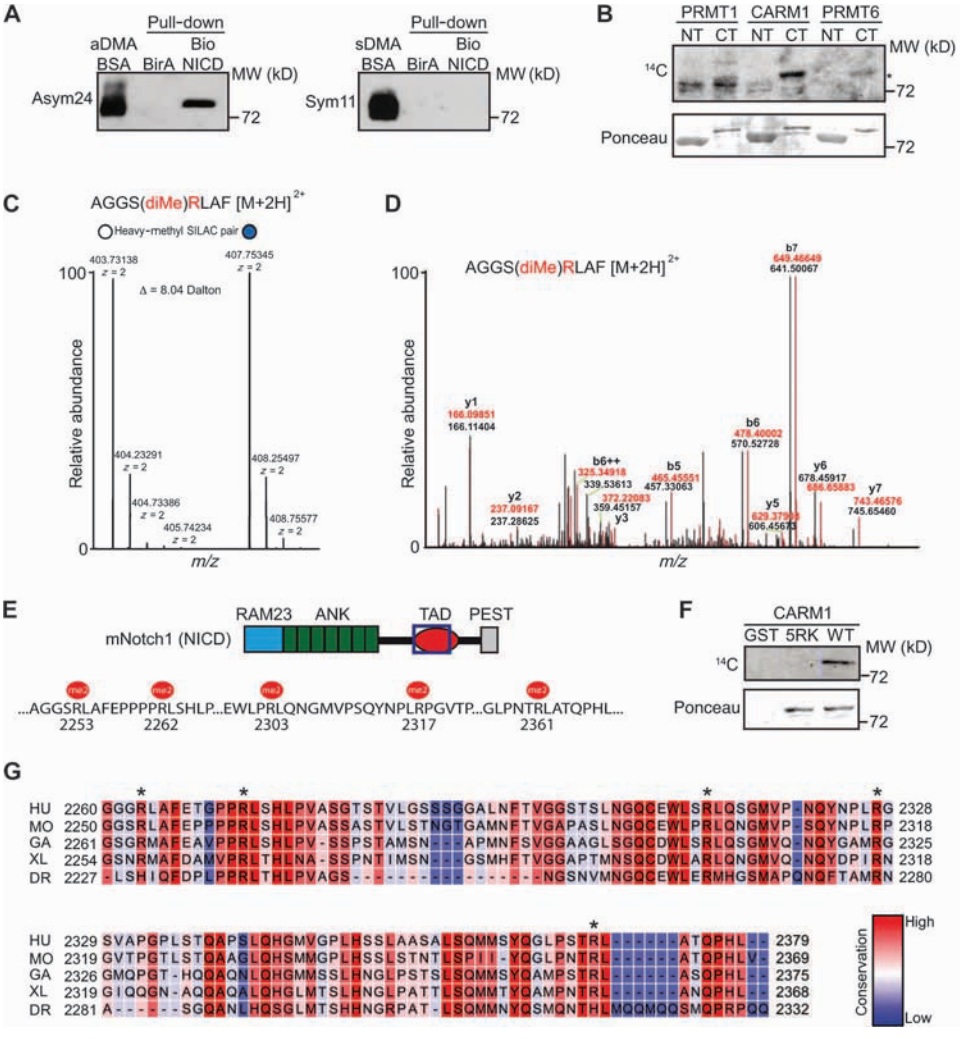

Fig. 1. CARM1 methylates the NICD at five conserved Arg residues in the TAD. (**A**) Streptavidin pull-down of biotin-tagged NICD (Bio-NICD) from Beko cells and blotted for asymmetrically (Asym24) or symmetrically (Sym11) dimethylated Arg. Biotin ligase–transfected Beko cells (BirA) and aDMA or sDMA coupled to BSA served as controls. (**B**) Autoradiography for in vitro methylation of GST-tagged NICD C- or N-terminal (CT, NT) fragments incubated with the indicated methyltransferase and ^{14}C-SAM (*S*-adenosyl-L-[methyl-^{14}C] methionine). Ponceau stain shows input. *, methylated bands. (**C**) Heavy methyl SILAC pair for Arg^{2253} in FLAG-NICD purified by FLAG immunoprecipitation from transiently transfected 293 cells showing the difference in molecular weight upon dimethylation. White circle marks unlabeled spectrum; blue circle marks heavy methyl SILAC–labeled spectrum. *m/z*, mass/charge ratio. (**D**) Collision-induced dissociation MS/MS spectrum of the peptide containing methylated Arg^{2253}. The spectrum is an overlay of the fragment ions generated from the unlabeled (black) and heavy methyl SILAC–labeled (red) peptide ion. (**E**) Schematic of murine Notch1 ICD domains and localization (blue outline) of the five methylated Arg in the TAD. (**F**) In vitro methylation of wild-type (WT) or mutant (5RK) GST-tagged C-terminal NICD fragments incubated with CARM1 and ^{14}C-SAM. (**G**) Species alignment of the NICD TAD. HU, *Homo sapiens*, accession number P46531; MO, *Mus musculus*, Q01705; GA, *Gallus gallus*, F1N270; XL, *Xenopus laevis*, P21783; DR, *Danio rerio*, A0PGH6. *, methylated Arg residues. Spectra are representative of two experiments. Blots are representative of three experiments.

CARM1 (PRMT4), or PRMT6. To analyze whether one of these methyltransferases can methylate the NICD, we performed in vitro methylation assays using hemagglutinin (HA)– or FLAG-tagged enzymes purified from human embryonic kidney (HEK) 293 cells and glutathione *S*-transferase (GST)–fused NICD (either the N- or C-terminal fragment) purified from bacteria (Fig. 1B and fig. S1B). The active enzymes were incubated with N- and C-terminal GST-NICD deletion constructs. Autoradiography revealed activity of CARM1 and, to a much lesser extent, PRMT6 against the C-terminal part of the NICD. Regarding PRMT1, there were only unspecific background bands of different molecular weight (Fig. 1B).

The NICD is methylated at five conserved arginine residues in the transactivation domain

To identify the exact methylation sites and prove the occurrence of arginine methylation in vivo, we used heavy methyl SILAC (stable isotope labeling by amino acids in cell culture), a quantitative mass spectrometry (MS) approach designed to detect novel methylation sites (fig. S2A) (*26*). HEK 293 cells were grown in heavy or light medium (containing different isotope-labeled methionine) and transiently transfected with FLAG-tagged NICD and CARM1. Purified NICD was processed and analyzed by MS. Five methylated residues were identified, as exemplified in a tandem MS (MS/MS) spectrum of such a methylated peptides (Fig. 1, C and D), and all of them were found in the transactivation domain (TAD) of the NICD (Fig. 1E). All five arginine residues were present; heavy methyl SILAC paired with a specific difference of 8 daltons and were identified as being dimethylated (Fig. 1D and fig. S2, B to E). The sites are distributed over 108 amino acids in the TAD of Notch1 (Fig. 1E). A peptide containing two sites that are both present in the methylated state suggests that methylation of several arginine residues occurs within the same protein. To validate that the methylation observed in the in vitro methylation assay occurred at the sites identified by MS, we replaced all five arginine residues with lysine residues (5RK), which is chemically the most similar amino acid to arginine because it bears the same charge. Wild-type and mutant NICD proteins were subsequently incubated with purified CARM1 in in vitro methylation assays and analyzed by autoradiography. Wild-type NICD, but not the NICD-5RK mutant, was methylated (Fig. 1F), suggesting that there are no additional methylation sites present in the NICD.

Sequence alignment of Notch1 from different species reveals that the five methylated arginine residues that are methylated are highly conserved. Conservation for all five residues is observed from human to *Xenopus*

laevis (Fig. 1G), and most of them are also conserved in *Danio rerio*, whereas the methylated arginine residues are absent in *Drosophila melanogaster*. The five arginine residues are present only in Notch1 but not in Notch2, Notch3, or Notch4 (fig. S1C). Thus, the five arginine residues are well conserved between species and are specific for Notch1.

Endogenous NICD methylation is CARM1-dependent and occurs in the nucleus

To explore whether endogenous NICD is methylated in cells, we generated an antibody specific for asymmetrically dimethylated Arg^{2361} in NICD, here called me2a-NICD (Fig. 2A). The Arg^{2361} residue was chosen because of the high abundance of methylation detected at that site in the MS analysis and the interspecies conservation of the site. The antibody detected a band in HEK 293 cells overexpressing wild-type or FLAG-tagged NICD, but not FLAG-tagged NICD-5RK (Fig. 2B), demonstrating its specificity. In peptide competition assays, only the addition of an asymmetrically dimethylated peptide to the antibody solution abrogated recognition by me2a-NICD in dot blot experiments (fig. S1D). Consistent with our expectations, overexpressing CARM1 in HEK 293 cells increased the amount of methylated NICD (Fig. 2C), whereas overexpressing a catalytically deficient CARM1 mutant (R169A) (*24*) showed no visible effect on the degree of NICD methylation (Fig. 2C). The R169A CARM1 mutant has a different gel migration pattern because of the lack of the HA tag (Fig. 2C). Furthermore, treating HEK 293 cells with the methyltransferase inhibitors 5′-deoxy-5′-(methylthio) adenosine (MTA) and adenosine dialdehyde (Adox) decreased the abundance of methylated NICD below detection (Fig. 2D). We detected methylation of the endogenous NICD in Beko cells, a mouse leukemia pre–T cell line that is characterized by constitutively active Notch signaling (Fig. 2E), as well as in various other cell types including mouse embryonic fibroblasts (MEFs), the human kidney carcinoma cell line SKRC-17, and the human pancreatic carcinoma cell line Panc1 (Fig. 2F and fig. S1E). CARM1 overexpression increased the amount of NICD methylation in Beko cells (Fig. 2G), and fractionation experiments showed that most methylated NICD was found in the nuclear fraction (Fig. 2H). Together, our data reveal that CARM1 methylates endogenous NICD in live cells, and that this methylation may occur in the nucleus. Additionally, we detected *Carm1* mRNA in all adult mouse tissues tested (fig. S1F), suggesting that CARM1 is ubiquitously expressed.

CARM1 physically and functionally interacts with the NICD-coactivator complex and is found at enhancers in a Notch-dependent manner

To assess the physical association of CARM1 with Notch pathway components, we generated a stable Beko cell line that overexpressed CARM1, and we performed coimmunoprecipitation experiments. Both the endogenous transcription factor RBP-J (Fig. 3A) and endogenous NICD (Fig. 3B) copurified with CARM1, suggesting that CARM1 may interact with RBP-J and NICD. To explore the functional role of CARM1, we performed short hairpin RNA (shRNA)–mediated knockdown experiments in Beko cells, which have constitutively active Notch signaling (*27*), and analyzed the expression of endogenous Notch target genes and the methylation of endogenous NICD. Compared to controls, knocking down CARM1 (Fig. 3C) reduced the methylation of endogenous NICD (Fig. 3D) and decreased the expression of a subset of Notch target genes (Fig. 3E). To determine whether the decreased expression of Notch target genes was due to reduced methylation of NICD, we performed inducible expression experiments in Beko cells stably transfected with plasmids expressing either wild-type or mutant (5RK) NICD fused to the tamoxifen-inducible estrogen receptor (ER) ligand-binding domain (herein called NICD-ER), in which tamoxifen treatment induces nuclear translocation of the fusion protein. Cells were then treated simultaneously with the γ-secretase inhibitor *N*-[*N*-(3,5-Difluorophenacetyl)-L-alanyl]-S-phenylglycine *t*-butyl ester (DAPT) and tamoxifen. γ-Secretase inhibition reduced the expression of Notch target genes *Ptcra* and *Gm266*, and tamoxifen-induced expression of the methylation-defective NICD was less effective than the wild-type

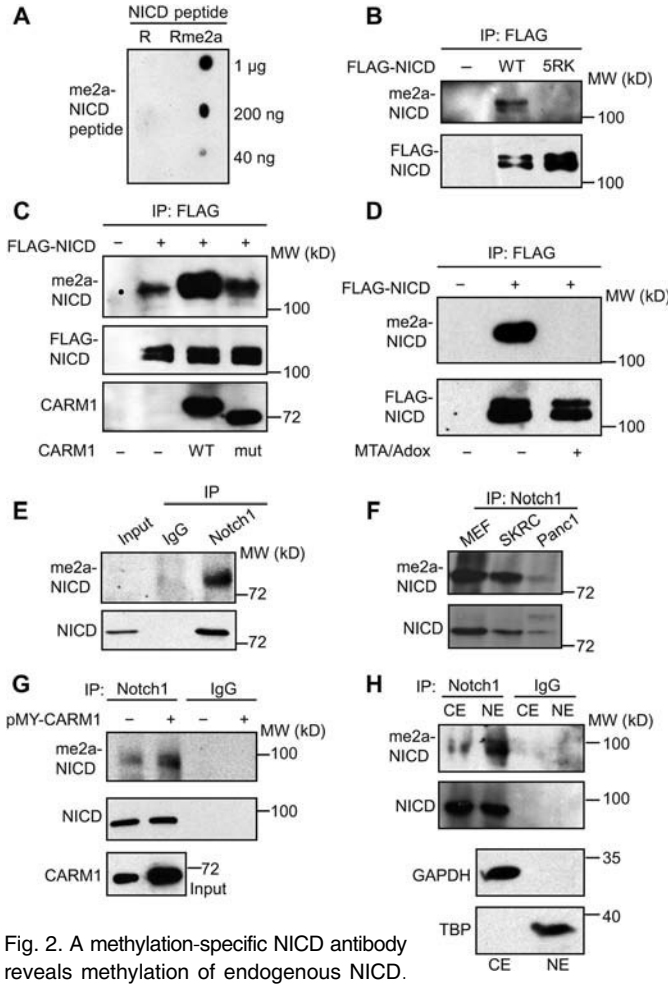

Fig. 2. A methylation-specific NICD antibody reveals methylation of endogenous NICD. (**A**) Dot blot analysis with unmodified (R, left) and asymmetrically dimethylated (Rme2a, right) peptide reveal specificity of the me2a-NICD antibody. (**B** and **C**) Pull-down [immunoprecipitation (IP)] and Western blotting for methylated NICD in 293 cells transfected with (B) WT or mutant (5RK) FLAG-tagged NICD or (C) FLAG-NICD and WT or catalytically deficient (mut: R169A) CARM1. (**D**) Pull-down and Western blotting for methylated NICD in 293 cells cotransfected with FLAG-NICD and HA and FLAG (HA/FLAG)–tagged CARM1 and treated with methyltransferase inhibitors MTA or Adox. (**E** and **F**) Pull-down (IP) for the intracellular domain of Notch1 (antibody: cleaved Notch1) and Western blotting for methylated, endogenous NICD in (E) Beko cells or (F) MEFs, renal carcinoma SKRC-17 cells (SKRC), and pancreatic cancer Panc1 cells. (**G**) As in (E) and (F), in Beko cells overexpressing CARM1. (**H**) Pull-down for the intracellular domain of Notch1 (antibody: bTan20-Notch1) and blotting for methylated NICD in the nuclear (NE) or cytoplasmic (CE) extract in Beko cells. GAPDH (glyceraldehyde-3-phosphate dehydrogenase), cytoplasmic marker; TBP (TATA-binding protein), nuclear marker. All blots are representative of at least two experiments.

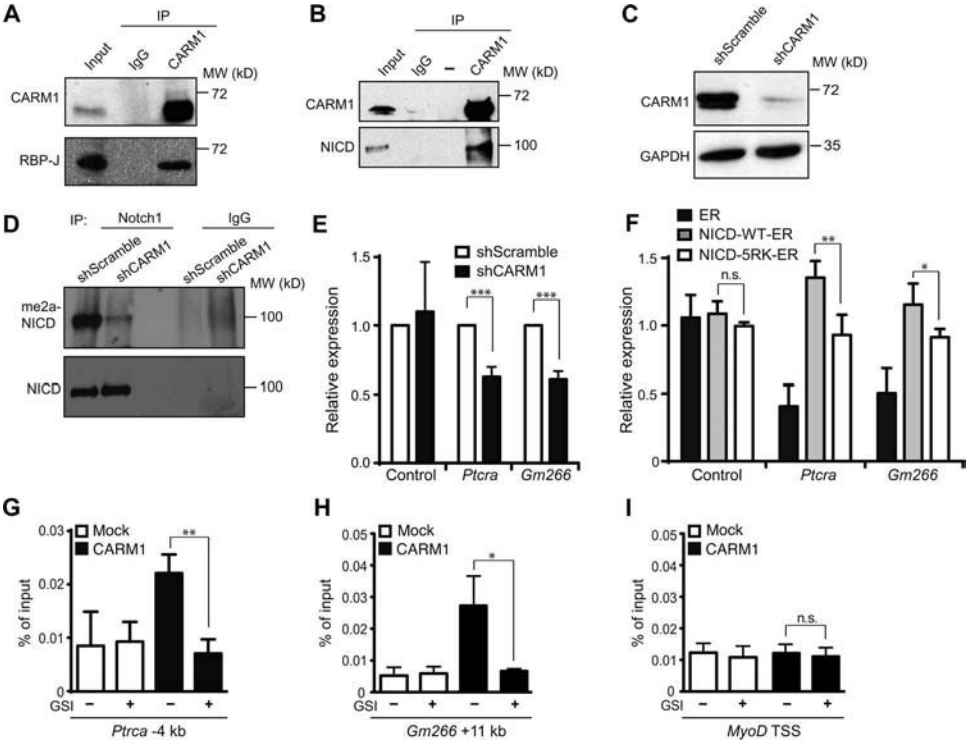

Fig. 3. Physical and functional interaction of CARM1 with the NICD-coactivator complex. (A and B) Pull-down of RBP-J (A) and Notch1 (B) with CARM1 immunoprecipitates from Beko cells transfected with a CARM1 expression plasmid. (C) Western blot for CARM1 in Beko cells transfected with control (Scramble) or CARM1-targeted shRNA. (D) Pull-down for cleaved Notch1 and Western blotting for methylated NICD in Beko cells transfected with control or CARM1 shRNA. (E) Expression of Notch target genes *Ptcra* and *Gm266* in Beko cells transfected with control (Scramble) or CARM1 shRNA. Control gene: *Hprt*. ***, $P = 0.0008$ (*Ptcra*) and $P = 0.0004$ (*Gm266*). (F) Expression of Notch target genes *Ptcra* and *Gm266* in Beko cells treated with the γ-secretase inhibitor DAPT and transfected with tamoxifen-inducible vector (ER), empty or encoding WT or mutant (5RK) NICD. Control, *GusB*. Expression was normalized to *Tbp*. *$P = 0.0123$; **$P = 0.0012$; n.s., not significant. (G to I) ChIP detection of CARM1 at Notch1/RBP-J binding sites in *Ptcra* (G), *Gm266* (H), or the *MyoD* transcriptional start site (TSS) (I) in Beko cells that were either unperturbed or treated with the γ-secretase inhibitor (GSI) DAPT. Protein A beads served as a binding control (mock). *$P = 0.0189$, **$P = 0.004$. Blots are representative of at least two experiments. Data are means ± SD from at least three experiments.

NICD at restoring expression of both genes (Fig. 3F), suggesting that methylation of NICD may promote a more effective Notch-induced transcriptional effect.

In a previously reported microarray analysis (*27*), treating Beko cells with the γ-secretase inhibitor DAPT suppressed the expression of Notch target genes, including *Ptcra* and *Gm266* (fig. S3A). To confirm NICD binding and investigate whether CARM1 is localized at RBP-J–Notch binding sites in these Notch target genes, we performed chromatin immunoprecipitation (ChIP) in transfected Beko cells. In cells expressing a Bio-NICD, we detected NICD at several enhancer sites of known Notch target genes, including *Ptcra*, *Gm266*, *Nrarp*, *CD25*, and *Hes1* (fig. S3B), which agrees with previously reported ChIP-sequencing data (*28*, *29*). In cells expressing CARM1, we detected CARM1 at NICD-bound enhancer sites of several Notch target genes, of which the expression was impaired by CARM1 knockdown (Fig. 3E and fig. S3C), in particular *Ptcra* (Fig. 3G), *Gm266* (Fig. 3H), *Hes1* (fig. S3D), and *CD25* (fig. S3E). In contrast, no CARM1 binding was observed at *Nrarp* (fig. S3F) or a control locus (Fig. 3I). CARM1 occupancy was lost upon treatment with the γ-secretase inhibitor DAPT (Fig. 3, E and F, and fig. S3, D and E), suggesting that the binding of CARM1 was dependent on active Notch signaling.

NICD protein stability is regulated by CARM1-dependent methylation

Phosphorylation (*4*–*6*), ubiquitination (*8*–*11*), and acetylation (*7*) influence the stability of NICD; therefore, we investigated whether methylation also affected its stability. Because mutating the five arginine residues to lysines in the methylation-defective NICD mutants (5RK) potentially introduces new ubiquitination sites, we generated a second mutant in which we mutated the five arginine residues to alanines (5RA) and tested the protein stability in HEK 293 cells in the presence of the protein synthesis inhibitor cycloheximide. Compared to the wild-type protein, degradation of the 5RA mutant protein was substantially slower (Fig. 4, A and B). In Beko cells, overexpressing CARM1 accelerated the degradation of endogenous Notch (fig. S4, A and B). To determine if this difference was due to CARM1-mediated NICD methylation, we used a fluorescence-activated cell sorting (FACS)–based approach in MEFs using a bicistronic vector expressing a green fluorescent protein (GFP) fused to either wild-type or 5RA mutant NICD together with an internal red fluorescent control (Tomato) (Fig. 4C). In wild-type MEFs, the stability of the nonmethylatable (5RA) NICD mutant was increased compared with that of the wild-type NICD protein, whereas in *CARM1*$^{-/-}$ MEFs, the stability of both constructs was similar (Fig. 4C), suggesting that increased turnover is indeed dependent on modification by CARM1 at these arginine residues. In HEK 293 cells overexpressing either wild-type or 5RA FLAG-tagged NICD, addition of the proteasome inhibitor *N*-carbobenzyloxy-L-leucyl-L-leucyl-L-leucinal (MG132) for 6 hours substantially increased the stability of the wild-type NICD protein, whereas there was little effect observed for the 5RA mutant (Fig. 4, D and E).

Additionally, NICD was phosphorylated in HEK 293 cells (fig. S4C). Phosphorylation of NICD triggers subsequent ubiquitination-dependent proteasomal degradation (*4*); therefore, our data suggest that the mutation of the arginine residues may impair proteasome-mediated degradation. Indeed, less ubiquitination was detected on the nonmethylatable mutant (5RA) NICD than the wild-type protein in HEK 293 cells cotransfected with HA-tagged ubiquitin (Fig. 4, F and G). We also observed that methylation coincided with phosphorylation because the me2a-NICD antibody preferentially recognized the upper, phosphorylated band of FLAG-NICD (fig. S4, C and D). Together, these data suggest that methylation promotes ubiquitin-dependent proteasomal degradation of NICD. Increased stability of the methylation-defective NICD was also inferred from a luciferase assay in HeLa cells expressing the Notch-dependent promoter construct pGA981/6 (*30*) together with a membrane-bound, truncated form of Notch1 that lacks a major portion of the extracellular domain, called N1ΔE, but is constantly cleaved into NICD by γ-secretase

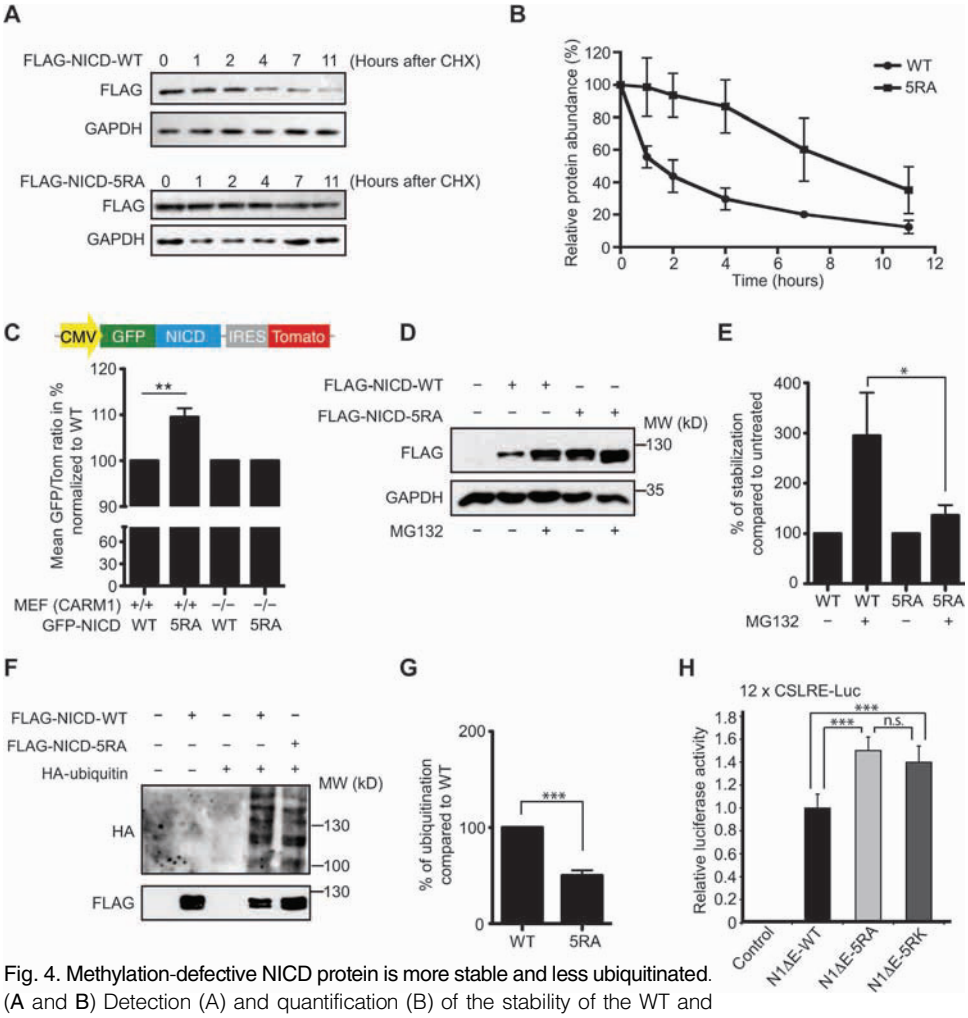

Fig. 4. Methylation-defective NICD protein is more stable and less ubiquitinated. (**A** and **B**) Detection (A) and quantification (B) of the stability of the WT and nonmethylatable mutant (5RA) FLAG-NICD protein in 293 cells treated with cycloheximide (CHX). The abundance of FLAG was normalized to GAPDH. (**C**) Schematic representation of the constructs used for the NICD stability assay in *CARM1*$^{+/+}$ and *CARM1*$^{-/-}$ MEFs transfected with either WT or mutant (5RA) GFP-tagged NICD. (**D** and **E**) Detection (D) and quantification (E) of the stability of FLAG-NICD proteins expressed in 293 cells treated for 6 hours with MG132. The abundance of FLAG signal was normalized to GAPDH. (**F** and **G**) Detection (F) and quantification (G) of ubiquitinated NICD in HEK 293 cells transfected as indicated. The HA signal was normalized to that of FLAG. (**H**) Luciferase assay in HeLa cells using the Notch-responsive promoter construct (12 × CSLRE-Luc) alone (control) or with the indicated expression construct (100 ng). Blots are representative of three experiments. Data are means ± SD from three or six (H) experiments. **P* = 0.0158, ***P* = 0.0012, ****P* < 0.0001.

activity and acts as a constitutively active form of Notch1 (*31*). Despite a much greater protein stability, expression of methylation-defective N1ΔE mutants (either 5RA or 5RK) increased the activation of a Notch1-dependent luciferase construct by only 1.2- to 1.5-fold compared to wild-type N1ΔE (Fig. 4H), suggesting that the mutants may have lower transcriptional activity.

Methylation-defective NICD shows decreased biological activity in *X. laevis* and zebrafish

Next, we tested the function of the N1ΔE-5RA mutant in *X. laevis* during embryonic development. Injection of mRNA encoding constitutively active, truncated wild-type Notch1 (N1ΔE-WT) decreased the abundance of N-tubulin, a marker for neurogenesis (Fig. 5, A and B). Although N-tubulin abundance at the same neurula stage (stage 15) was slightly reduced after injection of mRNA encoding the methylation-deficient, truncated mutant (N1ΔE-5RA), activation of Notch target genes was less pronounced compared with that induced by injection of the wild-type mRNA (Fig. 5C). In a later stage (stage 42), embryos injected with wild-type N1ΔE showed developmental defects that were also reported previously: smaller eyes, smaller components of the jaw (Meckel's cartilage, palatoquadrate, and ceratohyale), deformation of the intestine, smaller branchial arches, and edemas in the heart region (*32*). The incidence of defects was significantly less in embryos injected with the methylation-deficient mutant N1ΔE than in embryos injected with the wild-type construct (Fig. 5, D and E). Because these defects are the results of aberrant Notch activity in early development, differences in Notch target gene expression were no longer observed anymore at this late developmental stage (Fig. 5F).

To analyze the role of methylation of NICD in a second in vivo system, we overexpressed the wild-type or nonmethylatable truncated Notch1 construct by injecting the mRNA produced from the respective expression vectors (N1ΔE-WT, N1ΔE-5RK, and N1ΔE-5RA) into one-cell-stage zebrafish embryos. To confirm protein abundance and activity after mRNA injection, we co-injected a reporter plasmid that expresses GFP under the control of a Notch-dependent promoter (Fig. 5G). Endogenous NICD was not able to clearly induce GFP expression in zebrafish relative to that induced by the overexpressed N1ΔE mRNAs at 24 hours post-fertilization (hpf). As observed with *X. laevis* embryos, zebrafish embryos injected with wild-type N1ΔE at the one-cell stage showed severely impaired development of eye and brain structures at 24 hpf, whereas a significantly lower number of embryos injected with N1ΔE-5RK or N1ΔE-5RA displayed impaired formation of eyes and brain (Fig. 5, G and H).

In both *Xenopus* and zebrafish, expression of the constitutively active N1ΔE construct caused developmental defects (Fig. 5, E and H). However, animals expressing the nonmethylatable form had a significantly lower incidence of these defects than those expressing the wild-type form. This agrees with our Notch target gene expression data in vivo (Fig. 5C) and in cells (Fig. 3, E and F), suggesting that methylation-deficient NICD induces a dampened transcriptional effect.

Mathematical modeling suggests that wild-type but not methylation-defective NICD exhibits a sharp and punctuated Notch response

The apparent inconsistencies between our results [NICD stability (Fig. 4, A and B), transcriptional activity in reporter gene assays (Fig. 4H), and

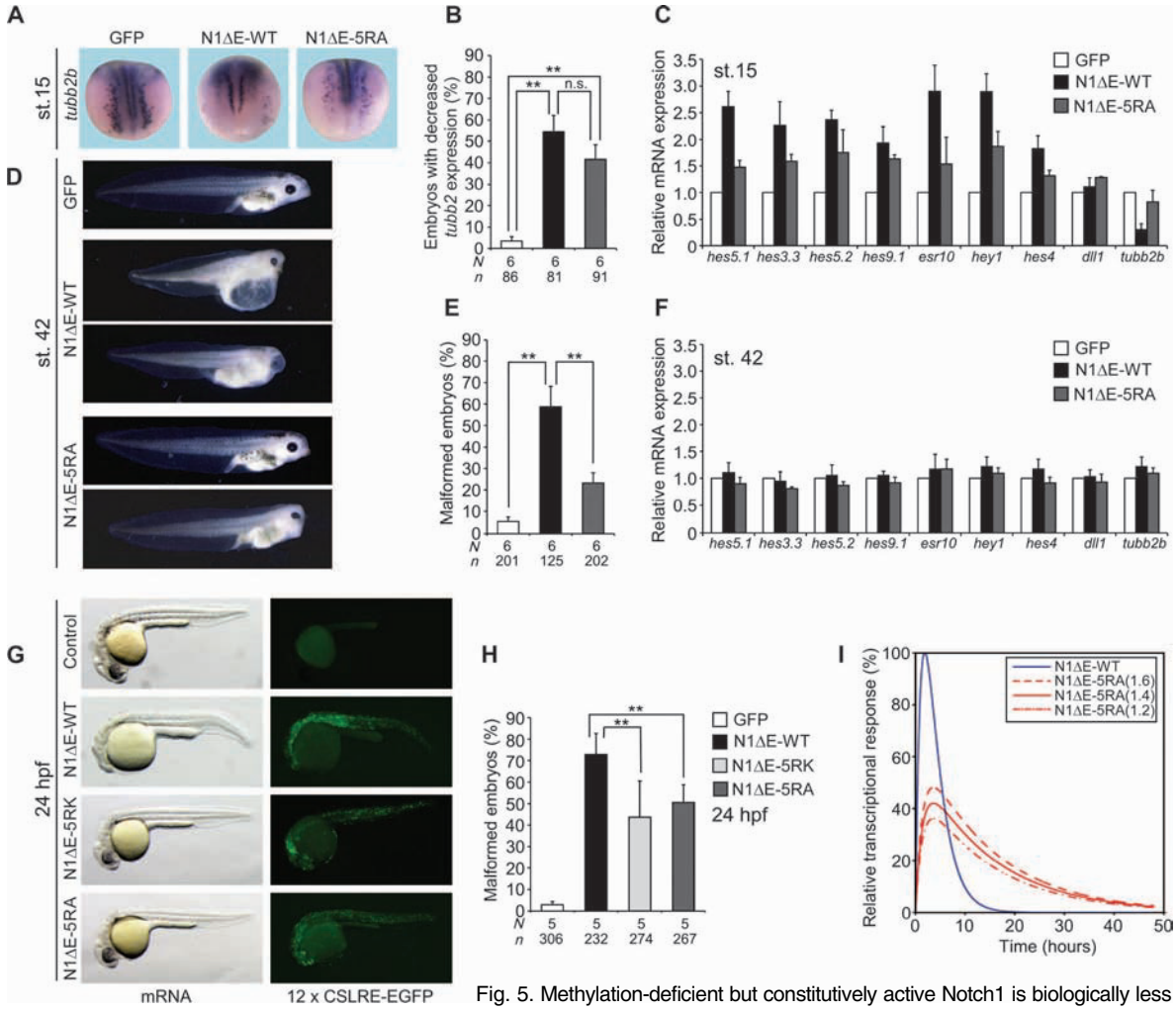

Fig. 5. Methylation-deficient but constitutively active Notch1 is biologically less active than its WT counterpart. (**A** to **C**) Detection and quantification of the primary neurogenesis marker *tubb2b* (A and B) and Notch target genes (C) in stage (st.) 15 *X. laevis* embryos injected with mRNA encoding constitutively active WT or methylation-deficient N1ΔE. (**D** to **F**) Images (D), the number with developmental defects (E), and Notch target gene expression (F) at developmental stage 42 in *X. laevis* embryos injected with the indicated mRNA. (**G** and **H**) Images at 24 hpf (G) and the number with developmental defects (H) in zebrafish embryos injected with the indicated mRNA. Co-injection of a Notch activity–dependent EGFP reporter plasmid was used to monitor the translation of the injected mRNA (G, right). Data in (C) and (F) are means ± SD from four experiments. Data in (B), (E), and (H) are means ± SD of the total number of embryos analyzed (*n*) in five or six independent experiments (*N*). $^{**}P < 0.001$ by nonparametric Mann-Whitney rank sum test. (**I**) Mathematical model predicting the dynamics of Notch-dependent transcriptional activation as a function of methylation-regulated stability of the NICD. Numbers in the legend alongside mutant simulations (red lines) refer to the relative transcriptional activity of these mutants in the luciferase assay (Fig. 4H).

in vivo activity (Fig. 5, A to H)] prompted us to develop an ordinary differential equation model for Notch target gene activation. This model (Fig. 5I) integrates wild-type or methylation-defective NICD protein stability and transcriptional output in our data combined with known dissociation constants between NICD and RBP-J (table S5). The interaction between RBP-J and wild-type NICD or methylation-defective NICD was similar (fig. S4E). Although the net result of transcription was slightly enhanced by expression of the methylation-defective NICD protein compared to a wild-type NICD protein (Fig. 4H), the stability of a mutant protein was significantly increased (Fig. 4, A and B). Our mathematical model revealed a differential Notch response. Whereas the wild-type NICD produces a short strong pulse, the methylation-defective NICD results in a flattened but prolonged response (Fig. 5I). This generic single-cell model captures the principal dynamic behavior of the Notch transcriptional response with or without methylation of NICD. It also generalizes to the in vivo situation because it shows significantly reduced phenotypes on a different time scale.

DISCUSSION

Our mathematical model suggests that Notch methylation is indispensable for the control of amplitude and duration of the Notch response ensuring accurate timing of Notch target gene transcription. This may play a crucial role in T cell development; *CARM1* knockout mice display a cell-intrinsic severe phenotype in T cell development and in fetal hematopoiesis (*24*, *33*). This is in line with a recent report that Notch1 signaling in

Notch1 hypomorphic mice is required for fetal hematopoietic stem cells (*34*). We detected *Carm1* mRNA in all adult mouse tissues tested, suggesting ubiquitous expression. CARM1 was shown to be dysregulated in colorectal and prostate cancer (*35*–*37*). In addition, CARM1 overexpression correlates with tumor grade in invasive mamma carcinoma (*38*), indicating that CARM1 expression might be a prognostic marker for breast cancer. In the context of diabetic nephropathy, CARM1 and Notch1 have been already linked (*39*). Regarding expression of CARM1 during development, the temporal expression patterns were analyzed in *X. laevis* and *Xenopus tropicalis* (*40*). CARM1 transcripts are maternally present and continuously increase from stage 10 (early gastrulation) to stage 33 (late tadpole). In zebrafish, *carm1* is already expressed at the two-cell stage, indicating its maternal distribution and necessity during early development. During further embryogenesis (at 6, 14, and 24 hpf), *carm1* mRNA is ubiquitously distributed with pronounced expression in the somites and anterior neural structures (*41*). At 48 and 72 hpf, *carm1* expression is more restricted to the ventricular system of the developing zebrafish brain and specific regions of the retina (*42*).

Regarding the methylation sites within the Notch1 protein, there are human disease–associated arginine mutations found either directly in the residues or in neighboring residues that cause frameshifts that effectively delete the arginine residues (table S1). In line with this, the pathophysiological and, most recently, physiological roles of Notch1-TAD were already elucidated in mice: A retroviral Notch1 mutant that lacks the TAD (Δ-TAD) fails to induce T cell leukemia in bone marrow transplantation experiments (*43*), and Δ-TAD within the endogenous Notch1 locus causes a severe defect in fetal hematopoiesis and heart development (*34*). NICD1-Δ-TAD protein is more stable than wild- type NICD, but transcriptional activation of a subset of Notch target genes is repressed (*34*). The observed link between transcriptional activation and protein turnover is similar to the mechanism proposed for c-Myc protein. Here, the c-Myc-TAD also harbors the degron sequence and promotes its own proteasomal degradation (*44*, *45*). This overlap between TAD and degron sequences is also valid for a significant number of other potent transcriptional activators such as E2F-1, c-Fos, GCN4, or p53 (*46*). In the case of Notch1, the degron sequence is localized in the C-terminal PEST domain that is central for the stability of the NICD and is a substrate for the E3 ubiquitin ligase FBXW7. The crosstalk between NICD arginine methylation and other posttranslational modifications such as phosphorylation, acetylation, hydroxylation, and ubiquitination (*13*) needs to be further investigated. It remains to be seen whether CARM1-mediated Notch methylation plays a central role in Notch-dependent diseases, such as leukemia.

MATERIALS AND METHODS

Cells and cell culture

Mouse leukemia pre–T cells (Beko) were cultured in Iscove's modified Dulbecco's medium (Gibco) supplemented with 2% fetal bovine serum (FBS; Pan Biotech), nonessential amino acids (Gibco), Primatone (0.3 mg/ml), penicillin/streptomycin (Gibco), and insulin (5 mg/liter; Sigma). A Beko cell line was generated stably expressing a biotin ligase (BirA) (*25*). HEK 293 and HEK 293T cells, HeLa cells, Panc1 cells, and MEFs (a gift from M. Bedford) were cultured in Dulbecco's modified Eagle's medium (DMEM; Gibco) supplemented with 10% FBS (Pan Biotech) and penicillin/streptomycin. The renal cell carcinoma line SKRC-17 (provided by G. Ritter, Sloan Kettering Cancer Center) was cultured in RPMI (Gibco) supplemented with 10% FBS and penicillin/streptomycin. All cell lines were maintained at 37°C in 5% CO_2.

Reagents and pharmacological treatments

HEK 293 cells were treated with 20 μM MG132 (CalBiochem), 20 μM Adox (Sigma), 50 μM MTA (Sigma), or cycloheximide (150 μg/ml; CalBiochem). Beko cells were treated with 5 μM MG132, cycloheximide (50 μg/ml), 0.5 μM tamoxifen, or the γ-secretase inhibitor DAPT (10 μg/ml; Alexis). The chemicals' respective vehicles were used as controls. To inhibit protein degradation and enable detection of methylated NICD, cells were treated with MG132 for 6 hours before cell lysis.

Antibodies

This study used commercial antibodies against CARM1 (Millipore 09-818, Bethyl A300-419A), GAPDH (Abcam, ab8245), FLAG (Sigma M5, F4042), HA (Santa Cruz Biotechnology, sc-805), ASYM24 (Millipore, 07-414), SYM11 (Millipore, 07-413), RBP-J (Cosmo Bio Co.), TBP (Santa Cruz Biotechnology, N-12, sc-204), and two antibodies that recognize the intracellular domain of Notch1 [cleaved Notch1 (Cell Signaling Technology, Val^{1744}, 2421, D3B8 #4147) and bTan20 Notch1 antibody (Abcam)].

Plasmids and transfections

The mouse Notch1-specific constructs pcDNA-FLAG-NICD, pcDNA3-FLAG-N1ΔE pCS2-N1ΔE, and pcDNA3-N1ΔE-ΔRBP mutant and the luciferase-based reporter construct 12 × CSLRE-Luc (pGa981/6) were described previously (*30*, *32*). For construction of the NICD-5RK and NICD-5RA mutant expression plasmids, a mouse Notch1-specific, 755–base pair Nco I fragment was generated by gene synthesis (GENEART/Life Technologies) that contained the mutated codons and was inserted into pcDNA3-mNICD, pcDNA3-mN1ΔE, and pCS2-mN1ΔE using the Nco I restriction sites. The reporter plasmid 12 × CSLRE-EGFP was constructed by first digesting pGL3-basic (Promega) with Nco I/Xba I to cut out the luciferase complementary DNA (cDNA). The EGFP cDNA was amplified by polymerase chain reaction (PCR) and inserted into the vector to generate pGE-basic (table S2). Then, the Notch-responsive promoter fragment from pGA981/6 (*30*) was inserted into pGE-basic after Nco I/Klenow/Hind III digestion. pcDNA-HA-PRMT or pcDNA-HA-FLAG-PRMT constructs were a gift from the laboratory of R. Schneider. CARM1-mut (R169A) was cloned from pGEX-CARM1-mut (R169A) (provided by M. Bedford) through Eco RI/Not I digestion into pcDNA3.1. To produce the GST-NICD fusion plasmids, mouse NICD fragments were subcloned from pcDNA-FLAG-NICD into the pGEX6P1 in-frame with GST via Eco RI/Not I (CT) or Eco RI/Xho I (NT) restriction sites (table S2). For the GFP-NICD fusions, pCSGS vectors were provided by J. Lindner (MPI Freiburg), and wild-type NICD or NICD-5RA mutant was cloned in-frame with GFP using Sma I restriction sites (table S2). To generate the stable cell line expressing CARM1, CARM1 was cloned from mouse cDNA into the retroviral pMY-Bio-IRES-GFP vector in two steps: it was cloned first into the pLXSP-Bio vector using Bgl II/Not I, then into the pMY-IRES-GFP vector using Eco RI/Not I. From this vector, Bio-CARM1 was cloned into pcDNA3.1 using Eco RI/Not I. Generation of pMT123-HA-8×-ubiquitin was described previously (*47*). pMY-Bio-NICD (*25*), pMIGR-NICD-ER, and pMIGR-dnMAML-ER (*27*) were described previously. pMIGR-mNICD-WT-ER-IRES-GFP and pMIGR-mNICD-5RK-ER-IRES-GFP were created by amplification of wild-type or mutant (5RK) mNICD from pcDNA-FLAG-NICD constructs using PCR and cloned using Sal I/Xho I digestion-insertion into pMIGR-ER-IRES-GFP.

Transient transfections of HEK 293 cells were performed with the calcium phosphate transfection method. MEFs were transfected using Lipofectamine 2000 (Invitrogen) according to the manufacturer's instructions. HeLa cells were transfected with the Nanofectin transfection reagent according to the manufacturer`s instructions (GE Healthcare). To generate stable Beko cell lines, we used the Phoenix retroviral packaging

cell line (ATCC) to produce viral supernatants, which were used in spin infections.

Luciferase assay

HeLa cells (5×10^4) were seeded in 24-well plates 24 hours before transient transfection. Transfection was performed using the Nanofectin reagent (see above) with 1 μg of reporter plasmid, either alone or together with 50 ng of NICD expression plasmid as indicated in the figure legend. Luciferase activity was determined 24 hours after transfection from at least four independent experiments with 20 μl of cleared lysate in an LB 9501 luminometer (Berthold), using the luciferase assay system from Promega.

X. laevis embryos, RNA microinjections, and whole-mount in situ hybridization

X. laevis embryos were obtained by in vitro fertilization, cultured, and staged as previously described (*48*). Experiments were performed in agreement with the German animal use and care law and were approved by the Regierungspräsidium Tübingen. GFP and N1ΔE mRNAs were obtained using the mMESSAGE mMACHINE SP6 Kit (Ambion) following the manufacturer's protocol after linearization of the pCS2 vectors with Kpn I (NEB). Embryos were injected at the two-cell stage bilaterally with 20 pg of mRNA into one blastomere for a total of 40 pg per embryo.

A digoxigenin-labeled antisense RNA probe of tubb2b was synthesized by restriction digestion and subsequent transcription with RNA polymerase (Roche). Injected embryos were fixed at stage 15 with MEMFA [0.1 M Mops (pH 7.4), 2 mM EGTA, 1 mM $MgSO_4$, 4% formaldehyde] overnight at 4°C. Whole-mount in situ hybridization was performed according to standard protocols (*49*). BM Purple (Roche) was used for staining. Afterward, embryos were refixed in MEMFA and bleached in 30% H_2O_2.

Zebrafish strains and injection procedures

Care and breeding of zebrafish (*D. rerio*) was conducted as described (*50*). The present study was performed after securing appropriate institutional approvals and conformed with the National Institutes of Health (NIH) *Guide for the Care and Use of Laboratory Animals*. For all injection procedures, the TE4/6 wild-type strain was used. Sense-capped RNA was synthesized using the mMESSAGE mMACHINE system (Ambion) as described above. mRNA was diluted (20 ng/μl in 0.2 M KCl) and co-microinjected with reporter plasmid (12 × CSLRE-EGFP; 10 ng/μl) into one-cell-stage embryos. Siblings from the same pool were injected using the reporter DNA as a control. Pictures were recorded at 24 hpf with an Olympus SZX16 stereomicroscope.

Mass spectrometry

To identify the Arg methylation sites on NICD, we used the heavy methyl SILAC approach (*26*). FLAG-NICD and HA/FLAG-CARM1 were overexpressed in HEK 293 cells. For five cell divisions, cells were cultured in light or heavy medium [DMEM containing unlabeled L-methionine or L-methionine-(methyl-$^{13}C^2H_3$) (15 mg/liter) and 10% dialyzed FCS]. As an internal control, the medium also contained light- or heavy-labeled L-lysine ($^2H_4$). Whole-cell extracts were prepared using CHAPS buffer. Equal amounts of heavy and light extracts were mixed, and the NICD was purified using an antibody against FLAG coupled to agarose beads (Sigma). Samples were loaded on an SDS–polyacrylamide gel electrophoresis (4 to 12% NuPAGE) gel and stained with colloidal Coomassie (Invitrogen). The band corresponding to FLAG-NICD was excised with a scalpel into cubes about 1 × 1 mm, and gel pieces were destained, dehydrated, and dried. Afterward, disulfide bonds were reduced with 10 mM dithiothreitol (DTT) and alkylated to prevent reoxidation. Then in-gel digestion with chymotrypsin was as previously described (*51*), stopped by the addition of trifluoroacetic acid (1% final concentration) followed by extraction of the peptides from the gel pieces. To desalt, clean, and concentrate the peptide mixture, homemade stop-and-go extraction (STAGE) tips were used (*52*). STAGE tip-eluted peptides were separated on-line to the mass spectrometer by using an Agilent nano-HPLC 1200 system. For each run, a 2.5-μl sample volume was applied with a loading flow rate of 0.5 μl/min. Peptides were eluted with a linear gradient of 10 to 60% buffer B (80% MeCN and 0.5% acetic acid) at a flow rate of 0.25 μl/min over 60 min. The nano–liquid chromatography system was coupled to a Thermo Fisher LTQ Orbitrap XL+ETD mass spectrometer, and MS data were acquired essentially as previously described (*53*) with the following modifications: The survey full-scan range was set to 350 to 2000 *m/z*, and each sample was measured in triplicates using a "Top5" strategy with either collision-induced dissociation, electron transfer dissociation, or higher-energy collisional dissociation fragmentation. Raw files were processed using the DTASuperCharge program of the MSQuant software suite, version 2.0b7 (*54*). Peak lists were searched by MASCOT (version 2.2, Matrix Science) against the IPI mouse database (version 3.65) combined with frequently observed contaminants and concatenated with the reversed versions of all sequences. Fixed and variable modifications were set as previously described (*26*). Protein and peptide identifications were further analyzed and manually verified by inspection of chromatograms and spectra.

Lentiviral shRNA knockdown

CARM1 knockdown was performed with the pLK0.1 Harvard shRNA library using a combination of targeted sequences against CARM1 (CCCTTAGCTAACACAGGGATT and CCACGATTTCTGTTCTTTCTA) or a scrambled shRNA as a control. HEK 293T cells were transfected using 30 μl of Lipofectamine 2000 reagent (Invitrogen) with the shRNA construct and the packaging vectors psPAX and pMD2G. After 48 hours of incubation, the supernatant from HEK 293T cells was used for spin infection of Beko cells, which were afterward selected by adding puromycin (2 μg/ml).

Cell extracts

Whole-cell extracts from HEK 293 cells were prepared by washing cells twice with ice-cold phosphate-buffered saline (PBS), then scraping them off and resuspending them in CHAPS buffer [50 mM tris-HCl (pH 7.8), 300 mM NaCl, 0.01 M CHAPS, 2 mM EDTA]. After 15 min of incubation on ice and vortexing for 15 s, lysates were centrifuged for 15 min at 14,000 rpm at 4°C. Alkaline phosphatase (NEB) was added to the cell extract, and the mixture was incubated for 1 hour at 37°C. To isolate the nuclear extract from Beko cells, 40 million cells were washed twice with PBS, and the pellet was resuspended in 1 ml of ice-cold hypotonic buffer [20 mM Hepes, 20 mM NaCl, 5 mM $MgCl_2$, 0.2 mM phenylmethylsulfonyl fluoride (PMSF), 1× protease inhibitors (Roche)], incubated 20 min on ice, and vortexed for 20 s. After a 2-min centrifugation at 14,000 rpm at 4°C, the pellet was washed once in PBS and resuspended in 200 μl of hypertonic buffer [20 mM Hepes, 300 mM KCl, 1 mM $MgCl_2$, 0.2% NP-40, 1 mM DTT, 1× protease inhibitors (Roche), and 0.2 mM PMSF]. After 20 min of incubation on ice, the lysate was cleared by centrifugation at 14,000 rpm for 5 min at 4°C. Protein concentrations were determined by Bradford assay (Bio-Rad), and extracts were analyzed by Western blot or used for immunoprecipitation.

Coimmunoprecipitation

The salt concentration of nuclear or whole-cell extracts was lowered, and preclearing was performed for 1 hour at 4°C with protein A beads. Antibodies or IgG control was added to the protein solutions and incubated in a cold room on a rotating wheel. Protein A beads were added to collect the protein-antibody complexes. After being washed, immunoprecipitated

proteins were analyzed by Western blot. Streptavidin pull-down was performed as described previously (*25*).

In vitro methylation assay

HA- or FLAG-tagged PRMTs were purified from HEK 293 cells. Cells were lysed in Ex-250 [20 mM Hepes (pH 7.9), 250 mM NaCl, 0.5% NP-40], and PRMTs were immunoprecipitated with HA antibody and protein G beads. After being washed, immunoprecipitated PRMTs were resuspended in PBS. Three micrograms of GST or GST-fusion proteins was incubated with 10 μl of immunoprecipitated PRMT enzymes. ^{14}C-SAM (0.5 μCi) was added, and the reaction was incubated for 90 min at 30°C. The samples were loaded on a gel, blotted onto a nitrocellulose membrane, and incubated with a radiosensitive film at −80°C before developing.

FACS-based stability assay

MEFs transfected with a bicistronic vector expressing a GFP-fusion construct and an internal red fluorescent control (tdTomato) (pCSGS-NICD-WT or pCSGS-NICD-5RA; see Fig. 4C) were acquired by FACS 24 hours after transfection using a FACSCalibur. The tdTomato fluorescence signal was used as a marker to identify transfected cells, whereas the GFP signal was used to monitor the expression of the GFP-NICD fusion proteins. The GFP/Tomato ratio was calculated using FlowJo software. The mean GFP/Tomato ratio for the peak representing MEFs transfected with wild-type GFP-NICD or GFP-NICD-5RA was calculated from three independent experiments, and the wild-type NICD GFP/Tomato ratio for each cell line was used as reference.

Cycloheximide chase assay

HEK 293 cells were transfected with an equal amount of the NICD-WT or NICD-5RA expression plasmid. After 36 hours, normal medium was replaced with medium containing cycloheximide (150 μg/ml). Samples were collected at the indicated time points, and whole-cell extracts were prepared and frozen immediately at –80°C. To monitor the degradation of endogenous NICD, 3×10^6 Beko cells per time point were seeded in a six-well plate, pretreated for 1 hour with cycloheximide (50 μg/ml), and then removed at the indicated time points for whole-cell extract preparation. Protein amounts were analyzed by Western blot and quantified with ImageJ software (NIH). NICD protein abundance was normalized to that of GAPDH.

In vivo ubiquitination

HEK 293 cells were cotransfected with expression plasmids encoding FLAG-NICD or HA-ubiquitin. Thirty-six hours after transfection, 20 μM MG132 was added and cells were washed twice with PBS 6 hours later. Cells were lysed in 300 μl of denaturing lysis buffer [20 mM tris-HCl (pH 7.4), 5 mM EDTA, 2% SDS, 10 mM DTT], and after incubation for 15 min at 99°C, the samples were diluted 10 times in immunoprecipitation buffer [50 mM tris-HCl (pH 7.4), 300 mM NaCl, 5 mM EDTA, 1% NP-40]. FLAG-NICD was immunoprecipitated with M2-FLAG–agarose beads (Sigma), and ubiquitination was analyzed after extensive washings with immunoprecipitation buffer and PBS by Western blotting with antibodies against the HA and FLAG tags.

Generation of an antibody against me2a-NICD

Antibody was raised against the asymmetrically dimethylated (R*) sequence CG-GLPNTR*LATQP (Biosyntan) in rabbit and affinity-purified with peptides immobilized on SulfoLink beads (Thermo Scientific, catalog no. 20401). The serum was first passed over a column with methylated NICD peptide; afterward, unspecific antibody was depleted over a column with unmethylated NICD peptide. The supernatant was saved as an antibody to me2a-NICD and dialyzed overnight against PBS. Specificity of the purified antibody was analyzed by dot blot. In competition assays, peptide (10 ng/ml) was added to the antibody solution and incubated for 30 min before incubation with the membrane.

Detection of methylated Notch1

To detect methylated Notch1, cells were treated for 6 hours with the proteasome inhibitor MG132. Cell extracts were prepared, and immunoprecipitation was performed with the antibody against cleaved Notch1 (Val^{1744}) (D3B8; Cell Signaling, #4147). Briefly, 200 μl of cell extract with a concentration of 1 μg/μl were precleared with protein A beads and afterward incubated with Notch1 antibody or rabbit IgG in a dilution of 1:200 overnight with rotation in a cold room. The next morning, 10 μl of protein A beads was added to precipitate the antibody-protein complexes for 1 hour, then washed four times with washing buffer (20 mM Hepes, 200 mM NaCl, 0.3% NP-40, 10% glycerol) and boiled for 5 min at 95°C in SDS loading buffer. Samples were loaded on a 6% acrylamide gel and then blotted onto a polyvinylidene difluoride membrane. The me2a-NICD antibody was diluted 1:1000 in 5% milk in tris-buffered saline with Tween 20 and incubated overnight at 4°C with the membrane.

Fractionation

To obtain clean cytoplasmic and nuclear fractions, we used a sucrose-based cell lysis buffer. Briefly, 1×10^8 Beko cells (previously treated for 6 hours with 5 μM MG132) were washed twice with ice-cold PBS and resuspended in 1 ml of sucrose buffer [20 mM Hepes (pH7.9), 250 mM sucrose, 10 mM KCl, 1.5 mM $MgCl_2$, 1 mM EDTA]; extraction of nuclei was confirmed by microscopy. After centrifugation for 5 min at 2000 rpm at 4°C, the supernatant was saved as the cytosolic fraction, and the pellet was washed twice with ice-cold PBS containing protease inhibitors and resuspended in 250 μl of buffer C [20 mM Hepes (pH 7.9), 300 mM NaCl, 1 mM $MgCl_2$, 0.1% NP-40, 20% glycerol] with micrococcus nuclease (Fermentas) and benzonase (Novagen). After 20 min of rotation in the cold room, the sample was spun down for 5 min at 14,000 rpm at 4°C, and the supernatant was saved as the nuclear extract. Protein concentration was determined, and both extracts were used to analyze the distribution of methylated Notch1 by immunoprecipitation and Western blotting.

Chromatin immunoprecipitation

ChIP assays were performed according to the Millipore protocol with a few modifications. Briefly, 20 million of Beko cells were fixed with 1% formaldehyde at room temperature for 15 min. Reaction was stopped by addition of 1:8 (v/v) of 1 M glycine, and cells were lysed in ChIP SDS lysis buffer [50 mM tris-HCl (pH 8.1), 10 mM EDTA, 1% SDS]. Chromatin was sheared using the Bioruptor (Diagenode). After preclearing, 5 μg of CARM1 antibody (Bethyl, A300-419A) was added, and the antibody complex was collected by adding 30 μl of protein A beads. Beads were washed once with low-salt buffer [20 mM tris-HCl (pH 8.1), 150 mM NaCl, 2 mM EDTA, 0.1% SDS, 1% Triton X-100], twice with high-salt buffer [20 mM tris-HCl (pH 8.1), 500 mM NaCl, 2 mM EDTA, 0.1% SDS, 1% Triton X-100], once with LiCl buffer [10 mM tris-HCl (pH 8.1), 250 mM LiCl, 1 mM EDTA, 1% NP-40], and finally twice with tris-EDTA (TE) buffer. DNA was purified, resuspended in TE buffer, and analyzed by quantitative real-time PCR (qPCR) using ChIP primers (table S3).

For the Bio-NICD ChIP, 28×10^6 Beko cells were first fixed for 1 hour in dimethyl adipimidate at room temperature and then for 30 min in 1% formaldehyde. After chromatin shearing in a Covaris S220 (28 cycles of 30 s on, 30 s off), chromatin was diluted, and preclearing was performed for 1 hour at 4°C with IgG magnetic beads M280 (Invitrogen, catalog no. 112.01D) blocked with salmon sperm DNA (10 mg/ml, Invitrogen) and fish skin

gelatin (Sigma-Aldrich, G7041). To precipitate Bio-NICD, 100 μg of chromatin was incubated overnight with streptavidin magnetic beads (M280 Invitrogen, catalog no. 112.06D). The next day, beads were washed two times with 1 ml of 150 mM NaCl washing buffer, two times with 1 ml of 500 mM NaCl washing buffer, and two times with 1 ml of TE. After removing the cross-linking, DNA was purified and resuspended in TE.

Inducible Notch switch-on/off system

Stable lines of Beko cells were created through retroviral infection with pMIGR-mNICD-WT-ER-IRES-GFP, pMIGR-mNICD-5RK-ER-IRES-GFP, or pMIGR-ER-IRES-GFP. Cells were sorted by FACS to obtain a defined low GFP–expressing population to achieve comparable expression and not to oversaturate promoters. Endogenous Notch signaling was then inhibited by adding DAPT (10 μg/ml) while simultaneously inducing the translocation of NICD-WT or NICD-5RK into the nucleus by adding 0.5 μM tamoxifen. As a control, cells were treated only with the vehicles DMSO and ethanol. After 8 hours, cells were harvested and total RNA was isolated as described below.

RNA extraction, reverse transcription, and qPCR

Total RNA was isolated using TRIzol reagents (Ambion, 15596018). For cDNA synthesis, 1 μg of RNA was reverse-transcribed using random hexamers and reverse transcriptase according to the manufacturer's protocol (Thermo Scientific, K1622). qPCRs were performed using Absolute QPCR ROX mix (Thermo Scientific, AB-1139) and gene-specific oligos and double-dye probes (Roche) and run in a 7300 ABI PRISM sequence detector system (Applied Biosystems) according to the manufacturer's recommendations. *X. laevis* samples were stored in RNAlater TissueProtect Tubes (Qiagen) until use, and mRNA abundance was assessed by quantitative reverse transcription PCR (RT-PCR). To determine mRNA expression, the SuperScript First-Strand Synthesis System for RT-PCR (Invitrogen) and SYBR Green PCR Master kit (Applied Biosystems) were used according to the manufacturer's instructions. The cDNAs were amplified with specific primers designed by using ProbeFinder software (Roche Applied Science). *hist1h4a* was used as a housekeeping gene for normalization. Primer sequences are shown in table S4. RNA isolation from adult mouse tissues and cDNA synthesis were described previously (*27*). QuantiTect Primer Assays (Qiagen) were used for subsequent qPCR of *HPRT* (QT00166768) and *CARM1* (QT00149170). In all cases, samples were tested at least in triplicate, and qPCRs were run on a 7500 Real-Time PCR System (Applied Biosystems) following the manufacturer's protocol.

Microarray

For microarray analysis of wild-type Beko cells upon treatment with a γ-secretase inhibitor, cells were treated with inhibitor (2 μg/ml) or the solvent (DMSO) for 24 hours. For microarray array analysis upon induction of NICD-ER or DNMaml-ER, the cells were stably infected with retroviral vector containing the respective construct. After selection, cells were treated with 4-hydroxytamoxifen (0.75 μg/ml) or the solvent (ethanol) for 48 hours. The cells were collected, and mRNA was purified using the RNeasy Mini Kit (Qiagen). Microarrays were performed using the GeneChip Mouse Gene 1.0 ST Array (Affymetrix). The data were normalized using RMA (robust multichip average) and represented in the heatmap visualizing their expression changes (*55*).

Mathematical model integrating Notch protein stability and transcriptional activation

The mathematical model of the Notch pathway (Fig. 5I) was built on the basis of both published findings (*56*–*61*) and data in this study. The model is described in detail in the Supplementary Materials.

Statistical analysis

Statistical analysis was carried out with the GraphPad Prism 5 software. Unless indicated, the two-tailed unpaired Student's *t* test was applied. Differences were considered significant if $P \leq 0.05$

SUPPLEMENTARY MATERIALS

www.sciencesignaling.org/cgi/content/full/8/369/ra30/DC1

Methods: Assumptions, parameters, and numerical methods underlying the mathematical model integrating NICD stability and transcriptional activation.

Fig. S1. Arginine residues in NICD are asymmetrically dimethylated and *CARM1* mRNA is expressed in adult mouse tissues.

Fig. S2. Methylation sites identified by heavy methyl SILAC.

Fig. S3. Selection of direct Notch target genes in pre–T cells.

Fig. S4. Methylation of the NICD in the context of its stability, phosphorylation, and binding to RBP-J.

Table S1. Mutations at the methylated arginine or surrounding residues in Notch1.

Table S2. Cloning primers used in this study.

Table S3. ChIP primers used in this study.

Table S4. qPCR primers used in this study.

Table S5. Available dissociation constants between the domains of NICD and RBP found in the literature.

References (*62*–*74*)

REFERENCES AND NOTES

1. S. Artavanis-Tsakonas, M. D. Rand, R. J. Lake, Notch signaling: Cell fate control and signal integration in development. *Science* **284**, 770–776 (1999).
2. R. Kopan, M. X. Ilagan, The canonical Notch signaling pathway: Unfolding the activation mechanism. *Cell* **137**, 216–233 (2009).
3. K. G. Guruharsha, M. W. Kankel, S. Artavanis-Tsakonas, The Notch signalling system: Recent insights into the complexity of a conserved pathway. *Nat. Rev. Genet.* **13**, 654–666 (2012).
4. C. J. Fryer, J. B. White, K. A. Jones, Mastermind recruits CycC:CDK8 to phosphorylate the Notch ICD and coordinate activation with turnover. *Mol. Cell* **16**, 509–520 (2004).
5. M. Y. Chiang, M. L. Xu, G. Histen, O. Shestova, M. Roy, Y. Nam, S. C. Blacklow, D. B. Sacks, W. S. Pear, J. C. Aster, Identification of a conserved negative regulatory sequence that influences the leukemogenic activity of NOTCH1. *Mol. Cell. Biol.* **26**, 6261–6271 (2006).
6. T. Ishitani, T. Hirao, M. Suzuki, M. Isoda, S. Ishitani, K. Harigaya, M. Kitagawa, K. Matsumoto, M. Itoh, Nemo-like kinase suppresses Notch signalling by interfering with formation of the Notch active transcriptional complex. *Nat. Cell Biol.* **12**, 278–285 (2010).
7. V. Guarani, G. Deflorian, C. A. Franco, M. Kruger, L. K. Phng, K. Bentley, L. Toussaint, F. Dequiedt, R. Mostoslavsky, M. H. Schmidt, B. Zimmermann, R. P. Brandes, M. Mione, C. H. Westphal, T. Braun, A. M. Zeiher, H. Gerhardt, S. Dimmeler, M. Potente, Acetylation-dependent regulation of endothelial Notch signalling by the SIRT1 deacetylase. *Nature* **473**, 234–238 (2011).
8. C. Oberg, J. Li, A. Pauley, E. Wolf, M. Gurney, U. Lendahl, The Notch intracellular domain is ubiquitinated and negatively regulated by the mammalian Sel-10 homolog. *J. Biol. Chem.* **276**, 35847–35853 (2001).
9. E. J. Hubbard, G. Wu, J. Kitajewski, I. Greenwald, *sel-10*, a negative regulator of *lin-12* activity in *Caenorhabditis elegans*, encodes a member of the CDC4 family of proteins. *Genes Dev.* **11**, 3182–3193 (1997).
10. N. Gupta-Rossi, O. Le Bail, H. Gonen, C. Brou, F. Logeat, E. Six, A. Ciechanover, A. Israel, Functional interaction between SEL-10, an F-box protein, and the nuclear form of activated Notch1 receptor. *J. Biol. Chem.* **276**, 34371–34378 (2001).
11. J. O'Neil, J. Grim, P. Strack, S. Rao, D. Tibbitts, C. Winter, J. Hardwick, M. Welcker, J. P. Meijerink, R. Pieters, G. Draetta, R. Sears, B. E. Clurman, A. T. Look, *FBW7* mutations in leukemic cells mediate NOTCH pathway activation and resistance to γ-secretase inhibitors. *J. Exp. Med.* **204**, 1813–1824 (2007).
12. B. J. Thompson, S. Buonamici, M. L. Sulis, T. Palomero, T. Vilimas, G. Basso, A. Ferrando, I. Aifantis, The SCF^{FBW7} ubiquitin ligase complex as a tumor suppressor in T cell leukemia. *J. Exp. Med.* **204**, 1825–1835 (2007).
13. T. Borggrefe, R. Liefke, Fine-tuning of the intracellular canonical Notch signaling pathway. *Cell Cycle* **11**, 264–276 (2012).
14. H. Wang, C. Zang, X. S. Liu, J. C. Aster, The role of Notch receptors in transcriptional regulation. *J. Cell. Physiol.* **230**, 982–988 (2015).
15. M. T. Bedford, Arginine methylation at a glance. *J. Cell Sci.* **120**, 4243–4246 (2007).
16. C. Berthet, F. Guehenneux, V. Revol, C. Samarut, A. Lukaszewicz, C. Dehay, C. Dumontet, J. P. Magaud, J. P. Rouault, Interaction of PRMT1 with BTG/TOB proteins in cell signalling: Molecular analysis and functional aspects. *Genes Cells* **7**, 29–39 (2002).
17. M. T. Bedford, S. G. Clarke, Protein arginine methylation in mammals: Who, what, and why. *Mol. Cell* **33**, 1–13 (2009).
18. U. M. Bauer, S. Daujat, S. J. Nielsen, K. Nightingale, T. Kouzarides, Methylation at arginine 17 of histone H3 is linked to gene activation. *EMBO Rep.* **3**, 39–44 (2002).

19. M. Covic, P. O. Hassa, S. Saccani, C. Buerki, N. I. Meier, C. Lombardi, R. Imhof, M. T. Bedford, G. Natoli, M. O. Hottiger, Arginine methyltransferase CARM1 is a promoter-specific regulator of NF-κB-dependent gene expression. *EMBO J.* **24**, 85–96 (2005).
20. A. N. Iberg, A. Espejo, D. Cheng, D. Kim, J. Michaud-Levesque, S. Richard, M. T. Bedford, Arginine methylation of the histone H3 tail impedes effector binding. *J. Biol. Chem.* **283**, 3006–3010 (2008).
21. D. Chen, S. M. Huang, M. R. Stallcup, Synergistic, p160 coactivator-dependent enhancement of estrogen receptor function by CARM1 and p300. *J. Biol. Chem.* **275**, 40810–40816 (2000).
22. D. Chen, H. Ma, H. Hong, S. S. Koh, S. M. Huang, B. T. Schurter, D. W. Aswad, M. R. Stallcup, Regulation of transcription by a protein methyltransferase. *Science* **284**, 2174–2177 (1999).
23. N. Yadav, J. Lee, J. Kim, J. Shen, M. C. Hu, C. M. Aldaz, M. T. Bedford, Specific protein methylation defects and gene expression perturbations in coactivator-associated arginine methyltransferase 1-deficient mice. *Proc. Natl. Acad. Sci. U.S.A.* **100**, 6464–6468 (2003).
24. D. Kim, J. Lee, D. Cheng, J. Li, C. Carter, E. Richie, M. T. Bedford, Enzymatic activity is required for the in vivo functions of CARM1. *J. Biol. Chem.* **285**, 1147–1152 (2010).
25. C. Jung, G. Mittler, F. Oswald, T. Borggrefe, RNA helicase Ddx5 and the noncoding RNA SRA act as coactivators in the Notch signaling pathway. *Biochim. Biophys. Acta* **1833**, 1180–1189 (2013).
26. S. E. Ong, G. Mittler, M. Mann, Identifying and quantifying in vivo methylation sites by heavy methyl SILAC. *Nat. Methods* **1**, 119–126 (2004).
27. R. Liefke, F. Oswald, C. Alvarado, D. Ferres-Marco, G. Mittler, P. Rodriguez, M. Dominguez, T. Borggrefe, Histone demethylase KDM5A is an integral part of the core Notch–RBP-J repressor complex. *Genes Dev.* **24**, 590–601 (2010).
28. H. Wang, J. Zou, B. Zhao, E. Johannsen, T. Ashworth, H. Wong, W. S. Pear, J. Schug, S. C. Blacklow, K. L. Arnett, B. E. Bernstein, E. Kieff, J. C. Aster, Genome-wide analysis reveals conserved and divergent features of Notch1/RBPJ binding in human and murine T-lymphoblastic leukemia cells. *Proc. Natl. Acad. Sci. U.S.A.* **108**, 14908–14913 (2011).
29. A. S. Geimer Le Lay, A. Oravecz, J. Mastio, C. Jung, P. Marchal, C. Ebel, D. Dembele, B. Jost, S. Le Gras, C. Thibault, T. Borggrefe, P. Kastner, S. Chan, The tumor suppressor Ikaros shapes the repertoire of Notch target genes in T cells. *Sci. Signal.* **7**, ra28 (2014).
30. F. Oswald, B. Tauber, T. Dobner, S. Bourteele, U. Kostezka, G. Adler, S. Liptay, R. M. Schmid, p300 acts as a transcriptional coactivator for mammalian Notch-1. *Mol. Cell. Biol.* **21**, 7761–7774 (2001).
31. F. Oswald, U. Kostezka, K. Astrahantseff, S. Bourteele, K. Dillinger, U. Zechner, L. Ludwig, M. Wilda, H. Hameister, W. Knochel, S. Liptay, R. M. Schmid, SHARP is a novel component of the Notch/RBP-Jκ signalling pathway. *EMBO J.* **21**, 5417–5426 (2002).
32. S. A. Wacker, C. Alvarado, G. von Wichert, U. Knippschild, J. Wiedenmann, K. Clauss, G. U. Nienhaus, H. Hameister, B. Baumann, T. Borggrefe, W. Knochel, F. Oswald, RITA, a novel modulator of Notch signalling, acts via nuclear export of RBP-J. *EMBO J.* **30**, 43–56 (2011).
33. J. Li, Z. Zhao, C. Carter, L. I. Ehrlich, M. T. Bedford, E. R. Richie, Coactivator-associated arginine methyltransferase 1 regulates fetal hematopoiesis and thymocyte development. *J. Immunol.* **190**, 597–604 (2013).
34. D. M. Gerhardt, K. V. Pajcini, T. D'Altri, L. Tu, R. Jain, L. Xu, M. J. Chen, S. Rentschler, O. Shestova, G. B. Wertheim, J. W. Tobias, M. Kluk, A. W. Wood, J. C. Aster, P. A. Gimotty, J. A. Epstein, N. Speck, A. Bigas, W. S. Pear, The Notch1 transcriptional activation domain is required for development and reveals a novel role for Notch1 signaling in fetal hematopoietic stem cells. *Genes Dev.* **28**, 576–593 (2014).
35. H. Hong, C. Kao, M. H. Jeng, J. N. Eble, M. O. Koch, T. A. Gardner, S. Zhang, L. Li, C. X. Pan, Z. Hu, G. T. MacLennan, L. Cheng, Aberrant expression of CARM1, a transcriptional coactivator of androgen receptor, in the development of prostate carcinoma and androgen-independent status. *Cancer* **101**, 83–89 (2004).
36. Y. R. Kim, B. K. Lee, R. Y. Park, N. T. Nguyen, J. A. Bae, D. D. Kwon, C. Jung, Differential CARM1 expression in prostate and colorectal cancers. *BMC Cancer* **10**, 197 (2010).
37. K. Mathioudaki, A. Papadokostopoulou, A. Scorilas, D. Xynopoulos, N. Agnanti, M. Talieri, The *PRMT1* gene expression pattern in colon cancer. *Br. J. Cancer* **99**, 2094–2099 (2008).
38. H. Cheng, Y. Qin, H. Fan, P. Su, X. Zhang, H. Zhang, G. Zhou, Overexpression of CARM1 in breast cancer is correlated with poorly characterized clinicopathologic parameters and molecular subtypes. *Diagn. Pathol.* **8**, 129 (2013).
39. D. Kim, S. Lim, M. Park, J. Choi, J. Kim, H. Han, K. Yoon, K. Kim, J. Lim, S. Park, Ubiquitination-dependent CARM1 degradation facilitates Notch1-mediated podocyte apoptosis in diabetic nephropathy. *Cell. Signal.* **26**, 1774–1782 (2014).
40. I. Yanai, L. Peshkin, P. Jorgensen, M. W. Kirschner, Mapping gene expression in two *Xenopus* species: Evolutionary constraints and developmental flexibility. *Dev. Cell* **20**, 483–496 (2011).
41. J. Batut, C. Duboe, L. Vandel, The methyltransferases PRMT4/CARM1 and PRMT5 control differentially myogenesis in zebrafish. *PLOS One* **6**, e25427 (2011).
42. C. Thisse, B. Thisse, High-resolution in situ hybridization to whole-mount zebrafish embryos. *Nat. Protoc.* **3**, 59–69 (2008).
43. J. C. Aster, L. Xu, F. G. Karnell, V. Patriub, J. C. Pui, W. S. Pear, Essential roles for ankyrin repeat and transactivation domains in induction of T-cell leukemia by notch1. *Mol. Cell. Biol.* **20**, 7505–7515 (2000).
44. S. Y. Kim, A. Herbst, K. A. Tworkowski, S. E. Salghetti, W. P. Tansey, Skp2 regulates Myc protein stability and activity. *Mol. Cell* **11**, 1177–1188 (2003).
45. S. E. Salghetti, S. Y. Kim, W. P. Tansey, Destruction of Myc by ubiquitin-mediated proteolysis: Cancer-associated and transforming mutations stabilize Myc. *EMBO J.* **18**, 717–726 (1999).
46. S. E. Salghetti, M. Muratani, H. Wijnen, B. Futcher, W. P. Tansey, Functional overlap of sequences that activate transcription and signal ubiquitin-mediated proteolysis. *Proc. Natl. Acad. Sci. U.S.A.* **97**, 3118–3123 (2000).
47. M. Treier, L. M. Staszewski, D. Bohmann, Ubiquitin-dependent c-Jun degradation in vivo is mediated by the δ domain. *Cell* **78**, 787–798 (1994).
48. P. D. Nieuwkoop, J. Faber, Digitized images and developmental data. In *Normal Table of Xenopus Laevis (Daudin)* (Garland Publishing Inc., New York, 1994).
49. A. Hemmati-Brivanlou, D. Frank, M. E. Bolce, B. D. Brown, H. L. Sive, R. M. Harland, Localization of specific mRNAs in *Xenopus* embryos by whole-mount in situ hybridization. *Development* **110**, 325–330 (1990).
50. S. Just, I. M. Berger, B. Meder, J. Backs, A. Keller, S. Marquart, K. Frese, E. Patzel, G. J. Rauch, H. A. Katus, W. Rottbauer, Protein kinase D2 controls cardiac valve formation in zebrafish by regulating histone deacetylase 5 activity. *Circulation* **124**, 324–334 (2011).
51. A. Shevchenko, H. Tomas, J. Havlis, J. V. Olsen, M. Mann, In-gel digestion for mass spectrometric characterization of proteins and proteomes. *Nat. Protoc.* **1**, 2856–2860 (2006).
52. J. Rappsilber, Y. Ishihama, M. Mann, Stop and go extraction tips for matrix-assisted laser desorption/ionization, nanoelectrospray, and LC/MS sample pretreatment in proteomics. *Anal. Chem.* **75**, 663–670 (2003).
53. P. Tropberger, S. Pott, C. Keller, K. Kamieniarz-Gdula, M. Caron, F. Richter, G. Li, G. Mittler, E. T. Liu, M. Buhler, R. Margueron, R. Schneider, Regulation of transcription through acetylation of H3K122 on the lateral surface of the histone octamer. *Cell* **152**, 859–872 (2013).
54. P. Mortensen, J. W. Gouw, J. V. Olsen, S. E. Ong, K. T. Rigbolt, J. Bunkenborg, J. Cox, L. J. Foster, A. J. Heck, B. Blagoev, J. S. Andersen, M. Mann, MSQuant, an open source platform for mass spectrometry-based quantitative proteomics. *J. Proteome Res.* **9**, 393–403 (2010).
55. P. Pavlidis, W. S. Noble, Matrix2png: A utility for visualizing matrix data. *Bioinformatics* **19**, 295–296 (2003).
56. C. Del Bianco, J. C. Aster, S. C. Blacklow, Mutational and energetic studies of Notch 1 transcription complexes. *J. Mol. Biol.* **376**, 131–140 (2008).
57. D. R. Friedmann, R. A. Kovall, Thermodynamic and structural insights into CSL-DNA complexes. *Protein Sci.* **19**, 34–46 (2010).
58. D. R. Friedmann, J. J. Wilson, R. A. Kovall, RAM-induced allostery facilitates assembly of a Notch pathway active transcription complex. *J. Biol. Chem.* **283**, 14781–14791 (2008).
59. S. E. Johnson, M. X. Ilagan, R. Kopan, D. Barrick, Thermodynamic analysis of the CSL·Notch interaction: Distribution of binding energy of the Notch RAM region to the CSL β-trefoil domain and the mode of competition with the viral transactivator EBNA2. *J. Biol. Chem.* **285**, 6681–6692 (2010).
60. O. Y. Lubman, M. X. Ilagan, R. Kopan, D. Barrick, Quantitative dissection of the Notch: CSL interaction: Insights into the Notch-mediated transcriptional switch. *J. Mol. Biol.* **365**, 577–589 (2007).
61. M. X. Ilagan, S. Lim, M. Fulbright, D. Piwnica-Worms, R. Kopan, Real-time imaging of notch activation with a luciferase complementation-based reporter. *Sci. Signal.* **4**, rs7 (2011).
62. H. Wang, C. Zhang, L. Taing, K. L. Arnett, Y. J. Wong, W. S. Pear, S. C. Blacklow, X. S. Liu, J. C. Aster, NOTCH1–RBPJ complexes drive target gene expression through dynamic interactions with superenhancers. *Proc. Natl. Acad. Sci. U.S.A.* **111**, 705–710 (2014).
63. D. Castel, P. Mourikis, S. J. Bartels, A. B. Brinkman, S. Tajbakhsh, H. G. Stunnenberg, Dynamic binding of RBPJ is determined by Notch signaling status. *Genes Dev.* **27**, 1059–1071 (2013).
64. J. C. Lagarias, J. A. Reeds, M. H. Wright, P. E. Wright, Convergence properties of the Nelder–Mead simplex method in low dimensions. *SIAM J. Optim.* **9**, 112–147 (1998).
65. L. F. Shampine, M. W. Reichelt, The MATLAB ODE suite. *SIAM J. Sci. Comput.* **18**, 1–22 (1997).
66. Y. M. Zhu, W. L. Zhao, J. F. Fu, J. Y. Shi, Q. Pan, J. Hu, X. D. Gao, B. Chen, J. M. Li, S. M. Xiong, L. J. Gu, J. Y. Tang, H. Liang, H. Jiang, Y. Q. Xue, Z. X. Shen, Z. Chen, S. J. Chen, *NOTCH1* mutations in T-cell acute lymphoblastic leukemia: Prognostic significance and implication in multifactorial leukemogenesis. *Clin. Cancer Res.* **12**, 3043–3049 (2006).
67. D. Rossi, S. Rasi, G. Fabbri, V. Spina, M. Fangazio, F. Forconi, R. Marasca, L. Laurenti, A. Bruscaggin, M. Cerri, S. Monti, S. Cresta, R. Fama, L. De Paoli, P. Bulian, V. Gattei, A. Guarini, S. Deaglio, D. Capello, R. Rabadan, L. Pasqualucci, R. Dalla-Favera, R. Foa, G. Gaidano, Mutations of *NOTCH1* are an independent predictor of survival in chronic lymphocytic leukemia. *Blood* **119**, 521–529 (2012).

68. N. Agrawal, M. J. Frederick, C. R. Pickering, C. Bettegowda, K. Chang, R. J. Li, C. Fakhry, T. X. Xie, J. Zhang, J. Wang, N. Zhang, A. K. El-Naggar, S. A. Jasser, J. N. Weinstein, L. Trevino, J. A. Drummond, D. M. Muzny, Y. Wu, L. D. Wood, R. H. Hruban, W. H. Westra, W. M. Koch, J. A. Califano, R. A. Gibbs, D. Sidransky, B. Vogelstein, V. E. Velculescu, N. Papadopoulos, D. A. Wheeler, K. W. Kinzler, J. N. Myers, Exome sequencing of head and neck squamous cell carcinoma reveals inactivating mutations in *NOTCH1*. *Science* **333**, 1154–1157 (2011).
69. A. Gutierrez, T. Sanda, R. Grebliunaite, A. Carracedo, L. Salmena, Y. Ahn, S. Dahlberg, D. Neuberg, L. A. Moreau, S. S. Winter, R. Larson, J. Zhang, A. Protopopov, L. Chin, P. P. Pandolfi, L. B. Silverman, S. P. Hunger, S. E. Sallan, A. T. Look, High frequency of *PTEN*, *PI3K*, and *AKT* abnormalities in T-cell acute lymphoblastic leukemia. *Blood* **114**, 647–650 (2009).
70. M. Imielinski, A. H. Berger, P. S. Hammerman, B. Hernandez, T. J. Pugh, E. Hodis, J. Cho, J. Suh, M. Capelletti, A. Sivachenko, C. Sougnez, D. Auclair, M. S. Lawrence, P. Stojanov, K. Cibulskis, K. Choi, L. de Waal, T. Sharifnia, A. Brooks, H. Greulich, S. Banerji, T. Zander, D. Seidel, F. Leenders, S. Ansen, C. Ludwig, W. Engel-Riedel, E. Stoelben, J. Wolf, C. Goparju, K. Thompson, W. Winckler, D. Kwiatkowski, B. E. Johnson, P. A. Janne, V. A. Miller, W. Pao, W. D. Travis, H. I. Pass, S. B. Gabriel, E. S. Lander, R. K. Thomas, L. A. Garraway, G. Getz, M. Meyerson, Mapping the hallmarks of lung adenocarcinoma with massively parallel sequencing. *Cell* **150**, 1107–1120 (2012).
71. Cancer Genome Atlas Research Network, Integrated genomic analyses of ovarian carcinoma. *Nature* **474**, 609–615 (2011).
72. B. Westhoff, I. N. Colaluca, G. D'Ario, M. Donzelli, D. Tosoni, S. Volorio, G. Pelosi, L. Spaggiari, G. Mazzarol, G. Viale, S. Pece, P. P. Di Fiore, Alterations of the Notch pathway in lung cancer. *Proc. Natl. Acad. Sci. U.S.A.* **106**, 22293–22298 (2009).
73. H. J. Huh, S. H. Lee, K. H. Yoo, K. W. Sung, H. H. Koo, J. H. Jang, K. Kim, S. J. Kim, W. S. Kim, C. W. Jung, K. O. Lee, S. H. Kim, H. J. Kim, Gene mutation profiles and prognostic implications in Korean patients with T-lymphoblastic leukemia. *Ann. Hematol.* **92**, 635–644 (2013).
74. S. Breit, M. Stanulla, T. Flohr, M. Schrappe, W. D. Ludwig, G. Tolle, M. Happich, M. U. Muckenthaler, A. E. Kulozik, Activating *NOTCH1* mutations predict favorable early treatment response and long-term outcome in childhood precursor T-cell lymphoblastic leukemia. *Blood* **108**, 1151–1157 (2006).

Acknowledgments: We thank M. Krötschel, S. Fietzeck, C. Grubisic, P. Käse, S. Schirmer, E. Röttele, and R. Rittelmann for excellent technical assistance. We are grateful to M. Lachner (MPI Freiburg), B. D. Giaimo (JLU Giessen), and U. Bauer (IMT Marburg) for critical reading of the manuscript. **Funding:** This work was supported by the collaborative research grant TRR81 and the Heisenberg program (BO 1639/5-1) by the DFG (German Research Foundation), the Max Planck Society to T.B. Further support was provided by the DFG through a collaborative research grant to F.O., H.A.K., and S.J. (SFB 1074/A3, SFB 1074/Z1, and JU2859/1-2, respectively); by the BMBF (Federal Ministry of Education and Research, research nucleus SyStAR) to F.O., M.K., and H.A.K.; by the European Commission's Seventh Framework Program (FP7/2007–2013) under grant agreement 602783 to H.A.K.; the Boehringer Ingelheim Ulm University BioCenter (BIU) to S.J.; the Ministry of Science, Research, and Arts of the State of Baden-Wuertemberg, Germany, to F.O.; and the Medical Faculty of Ulm University ("Bausteinprogramm" to I.M.B.). W.C. was supported by the International Graduate School in Molecular Medicine, Ulm (GSC270). Additional support was provided by the Excellence Initiative of the German Federal and State Governments, EXC 294 in Freiburg and Excellence Cluster for Cardio Pulmonary System (ECCPS) in Giessen. **Author contributions:** K.H. designed and performed SILAC MS, most of the biochemical experiments (coimmunoprecipitation experiments, methylation assays, and Notch protein stability assays), ChIP, and knockdown experiments; analyzed the data; and wrote the manuscript. G.M. designed and performed MS experiments and analyzed the data. W.C. and M.K. performed *Xenopus* experiments and analyzed the data. F.F. performed Notch ChIP experiments. F.O. did the mouse tissue preparation and performed expression analysis and coimmunoprecipitation experiments. R.L. performed microarray experiments and analyzed the data. I.M.B. and S.J. performed zebrafish experiments and analyzed the data. J.E.S., H.A.K., and F.O. did the mathematical modeling. F.O. and T.B. designed experiments, analyzed the data, supervised all different parts of the project, and wrote the manuscript. **Competing interests:** The authors declare that they have no competing interests. **Data and materials availability:** The raw MS data are accessible at http://public.ie-freiburg.mpg.de/proteomics/tb0215. The microarray data have been deposited in the National Center for Biotechnology Information Gene Expression Omnibus, accession number GSE62528.

Submitted 11 September 2014
Accepted 20 February 2015
Final Publication 24 March 2015
10.1126/scisignal.2005892
Citation: K. Hein, G. Mittler, W. Cizelsky, M. Kühl, F. Ferrante, R. Liefke, I. M. Berger, S. Just, J. E. Sträng, H. A. Kestler, F. Oswald, T. Borggrefe, Site-specific methylation of Notch1 controls the amplitude and duration of the Notch1 response. *Sci. Signal.* **8**, ra30 (2015).

Site-specific methylation of Notch1 controls the amplitude and duration of the Notch1 response

Kerstin Hein, Gerhard Mittler, Wiebke Cizelsky, Michael Kühl, Francesca Ferrante, Robert Liefke, Ina M. Berger, Steffen Just, J. Eric Sträng, Hans A. Kestler, Franz Oswald and Tilman Borggrefe

(March 24, 2015)
Science Signaling **8** (369), ra30. [doi: 10.1126/scisignal.2005892]

Science Signaling
AAAS

www.sciencesignaling.org/cgi/content/full/8/369/ra30/DC1

Supplementary Materials for

Site-specific methylation of Notch1 controls the amplitude and duration of the Notch1 response

Kerstin Hein, Gerhard Mittler, Wiebke Cizelsky, Michael Kühl, Francesca Ferrante, Robert Liefke, Ina M. Berger, Steffen Just, J. Eric Sträng, Hans A. Kestler, Franz Oswald,* Tilman Borggrefe*

*Corresponding author. E-mail: tilman.borggrefe@biochemie.med.uni-giessen.de (T.B.); franz.oswald@uni-ulm.de (F.O.)

Published 24 March 2015, *Sci. Signal.* **8**, ra30 (2015)
DOI: 10.1126/scisignal.2005892

The PDF file includes:

SUPPLEMENTARY MATERIALS

Supplementary Methods: Assumptions, parameters, and numerical methods underlying the mathematical model integrating NICD stability and transcriptional activation.

Assumptions and differential equations for the core Notch pathway model

The model shown in Fig. 5I is based on the core constituents of the transcription-enabling complex, namely NICD, RBP-J and the corresponding DNA-binding sites (called LOCI herein). To avoid confusion, we shorten "RBP-J" to RBP in this section. We also do not take into account the role of Mastermind (MAML). We assume that it is ubiquitously present and that its binding is instantaneous. We focused on the core constituents of the transcription-enabling complex, namely NICD and RBP after NICD cleavage.

We assume intracellular transport processes as instantaneous; as such, the time between binding of NOTCH to its ligand on the cellular surface to the proteasomal degradation of NICD in the nucleus will be regarded as instantaneous. In the current setting this is of little importance, because we can focus on the actual onset of transcription rather than the activation of the NOTCH receptors, whereupon the time between the release of NICD in the nucleus and actual transcription is of larger importance.

The basic properties of the system are described with the help of measured dissociation constants (*56-63*) (table S5) and we further assume that the nuclear concentrations of respective cofactors are appropriate. In other words we assume that enough molecules are present and that those are properly mixed throughout the nucleus. In addition, we experimentally validated that the interaction of RBP with NICD mutants does not change (fig. S4E). Thus we assume that the interaction between RBP and NICD is unaffected by the considered mutations.

To represent the behavior of the system with a set of differential equations, the reactions need to be characterized by appropriate forward and reverse (dynamic) reaction rates. The reaction rates are scaled from the dissociation constants using the measurements reported previously (*61*). Their results show that the maximal concentration of the NICD-RBP complex will occur 2 to 3 hours after activation.

The system of ordinary equations was formulated using the flows corresponding to the following reversible reactions, each associated with its dissociation constant K:

$$NICD + RBP \underset{}{\overset{K_1}{\leftrightharpoons}} NICD|RBP$$

$$NICD|RBP + LOCI \underset{}{\overset{K_2}{\leftrightharpoons}} NICD|\mathrm{RBP}\,|\,\mathrm{LOCI}$$

$$RBP + LOCI \overset{K_3}{\leftrightharpoons} RBP|LOCI$$

Denoting the concentrations of each species by square brackets and introducing the shorthands, wherein [LOCI] stands for the effective concentration of free DNA-binding regions and *t* represents the time, we get:

$$n\,(t) = [\mathrm{NICD}](t), r\,(t) = [\mathrm{RBP}](t), (t) = [\mathrm{LOCI}](t), nr\,(t) = [\mathrm{NICD|RBP}](t)$$
$$rl\,(t) = [\mathrm{RBP|LOCI}](t), nrl\,(t) = [\mathrm{NICD|RBP|LOCI}]\,(t)$$

Upon introducing $k_{n\pm}$ as the reaction rates corresponding to the n^{th} dissociation constant and k the rate of degradation of NICD|RBP (the NICD-RBP complex), the corresponding set of differential equations are:

$$\frac{n}{t} = k_{1+} \cdot nr - k_{1-} \cdot n \cdot r$$
$$\frac{r}{t} = k_{1+} \cdot nr - k_{1-} \cdot n \cdot r + k_{2-} \cdot rl - k_{2+} \cdot r \cdot l$$
$$\frac{l}{t} = k_{3-} \cdot nrl - k_{3+} \cdot nr \cdot l + k_{2-} \cdot rl - k_{2+} \cdot r \cdot l$$
$$\frac{nr}{t} = k_{1-} \cdot n \cdot r - k_{1+} \cdot nr + k_{3+} \cdot nrl - k_{3-} \cdot nr \cdot l - k \cdot nr$$
$$\frac{rl}{t} = k_{2+} \cdot r \cdot l - k_{2-} \cdot rl$$
$$\frac{nrl}{t} = k_{3+} \cdot nr \cdot l - k_{3-} \cdot nrl$$

The initial conditions are given by the steady state values corresponding to $[\mathrm{NICD}]\,(t) = 0$. The system of equations is then solved with $[\mathrm{NICD}]\,(0) = n_0$, the induced amount of NICD is thus corresponding to an unstimulated Notch pathway responding to an induced activity at $t = 0$. The given system thus mimics the NICD induced activity of the Notch pathway under the above simplifying assumptions.

The transcription rates are then assumed to be proportional to the amount of NICD|RBP|LOCI which in turn is proportional to the concentration $[NICD|RBP|LOCI]$ since a constant nuclear volume is assumed. Assuming that the degradation rates for the transcripts are negligible, the quotient $Q(t)$ of transcripts amounts, $TRANS$, corresponding to the wild-type (wt) and methylation-defective mutant (5RA) forms accumulated up to time *t* will be given by:

$$Q(t) = \frac{\int_0^T TRANS_{wt}(t)dt}{\int_0^T TRANS_{5RA}(t)dt}$$

$$= \frac{\int_0^T \int_{nucleus} [\text{NICD}|\text{RBP}|\text{LOCI}]_{wt}\ dx^3 dt}{\int_0^T \int_{nucleus} [\text{NICD}|\text{RBP}|\text{LOCI}]_{5RA}\ dx^3 dt}$$

$$= \frac{k_{wt} \int_0^T [\text{NICD}|\text{RBP}|\text{LOCI}]_{wt}\ dt}{k_{mut} \int_0^T [\text{NICD}|\text{RBP}|\text{LOCI}]_{5RA}\ dt}$$

In the equation above, k_{mut} and k_{wt} denote the effective transcription rates of the mutated and wild-type forms of NICD, respectively. Having measured the quotient after some time T, and assuming that the system of differential equations approximates the evolutions of $[\text{NICD}|\text{RBP}|\text{LOCI}](t)$, it is hence possible to extrapolate $\frac{k_{wt}}{k_{mut}}$ the quotient of effective transcription efficiency. Choosing a large enough T further ensures that the effects due to transient behaviors neglected by the system of equations remain small.

Parameter modeling

When only considering the evolution of [NICD|RBP|LOCI], the principal difference for the dynamics for wild-type or methylation-defective mutant NICD is the ubiquitination/degradation rates. As our model describes the ubiquitination/degradation of NICD through NICD|RBP decay, we assumed, as experimentally measured in Fig. 4, A and B, that the corresponding free half-lives of 1.8 hours and 10 hours for wild-type NICD and mutated NICD forms, respectively:

$$k_{wt} = \frac{\ln(2)}{1.8}\ h^{-1}$$

$$k_{mut} = \frac{\ln(2)}{10}\ h^{-1}$$

All other parameters of the model were identical. As realistic values for the nuclear concentrations of RBP are not available, the quotient between the number of RBP and LOCI molecules/sites, q, was assumed to satisfy

$$10^2 \leq\ q\ \leq 10^3.$$

Similarly, no definitive figures for the number of DNA-binding regions per nucleus are known. The corresponding values, $ltot$, were assumed to lie in an interval including the values found in the literature (*62, 63*).

$$118 < ltot < 1.3 \times 10^4$$

As the measured dissociation constants showed some variability, the simulations were conducted for combinations of dissociation constants in the intervals spanned by the values found in the literature (table S5) up to $T = 24$ hours, the time at which transcription was measured.

$$14\ \text{nM} \leq K1 \leq 510\ \text{nM}$$

$$200\ \text{nM} \leq K2 \leq 300\ \text{nM}$$

$$200\ \text{nM} \leq K3 \leq 300\ \text{nM}$$

The corresponding reaction rates were extrapolated using the finding that a NICD|RBP peak will follow approximately 2.5 hours after Notch activation.

As the actual value of n_0 has little bearing on the output concentrations of NICD|RBP|LOCI compound (see below), n_0 was fixed at 100 nM. Additionally, we take into account variations in the cumulative transcriptional activity, as depicted in the luciferase assay (Fig. 4H), and assume the corresponding activity of the mutant 5RA construct amount takes values between 1.2 and 1.6 relative to the wild-type (1.0).

Numerical considerations

All simulations where conducted using MATLAB 2012b/2013a software (MathWorks Inc.). Optimizations were made using *fminsearch* the Matlab implementation of the Nelder-Mead algorithm (*64*). The system of differential equations was solved numerically by *ode15s*, a MATLAB solver for stiff equation systems (*65*). For each set of parameters, the system was started at equilibrium with $[\text{NICD}] = 0$. At $t = 0$, an amount, n_0 of NICD was introduced. The reaction rates were optimized in such a way that the maximum [NICD|RBP] was achieved after 2.5 hours after the NICD activation and that [NICD|RBP|LOCI] peaks after 10 hours. The reaction rates corresponding to K_1 and K_2 were defined by a single common scaling factor and those corresponding to K_3 by a second scaling factor.

As expected, the actual value of n_0 had no impact on the actual value of the quotient

$$\frac{\int_0^T [NICD|RBP|LOCI]_{wt}\, dt}{\int_0^T [NICD|RBP|LOCI]_{5RA}\, dt}$$

and was fixed to an arbitrary value of 100 nM. Simulations varying all parameters verified

that the actual value of n_0 was not of importance.

Subsequent simulations varying the two remaining parameters, namely $ltot$ and q, led us to conclude that:

$$0.19 < \frac{\int_0^T [NICD|RBP|LOCI]_{wt}\, dt}{\int_0^T [NICD|RBP|LOCI]_{5RA}\, dt} < 0.2$$

or equivalently:

$$0.19 < \frac{k_{mut}}{k_{wt}} \frac{k_{wt}}{k_{mut}} \frac{\int_0^T [\mathrm{NICD|RBP|LOCI}]_{wt}\, dt}{\int_0^T [\mathrm{NICD|RBP|LOCI}]_{5RA}\, dt} < 0.2,$$

$$0.19 < \frac{k_{mut}}{k_{wt}} Q(24 \text{ hours}) < 0.2. \quad (1)$$

As in the luciferase assay (Fig. 4H), we assume that the relative transcriptional activity by the mutant compared to the wild type is 1.4 ± 0.2:

$$1.2 < Q(24 \text{ hours}) < 1.6.$$

Insertion of Q into the first equation yields a transcription efficiency of:

$$0.11 < \frac{k_{mut}}{k_{wt}} < 0.2.$$

In other words, the transcriptional activity of the wild-type NICD is 6 to 8.5 times larger than its mutant equivalent under the above assumptions.

Supplementary Figures

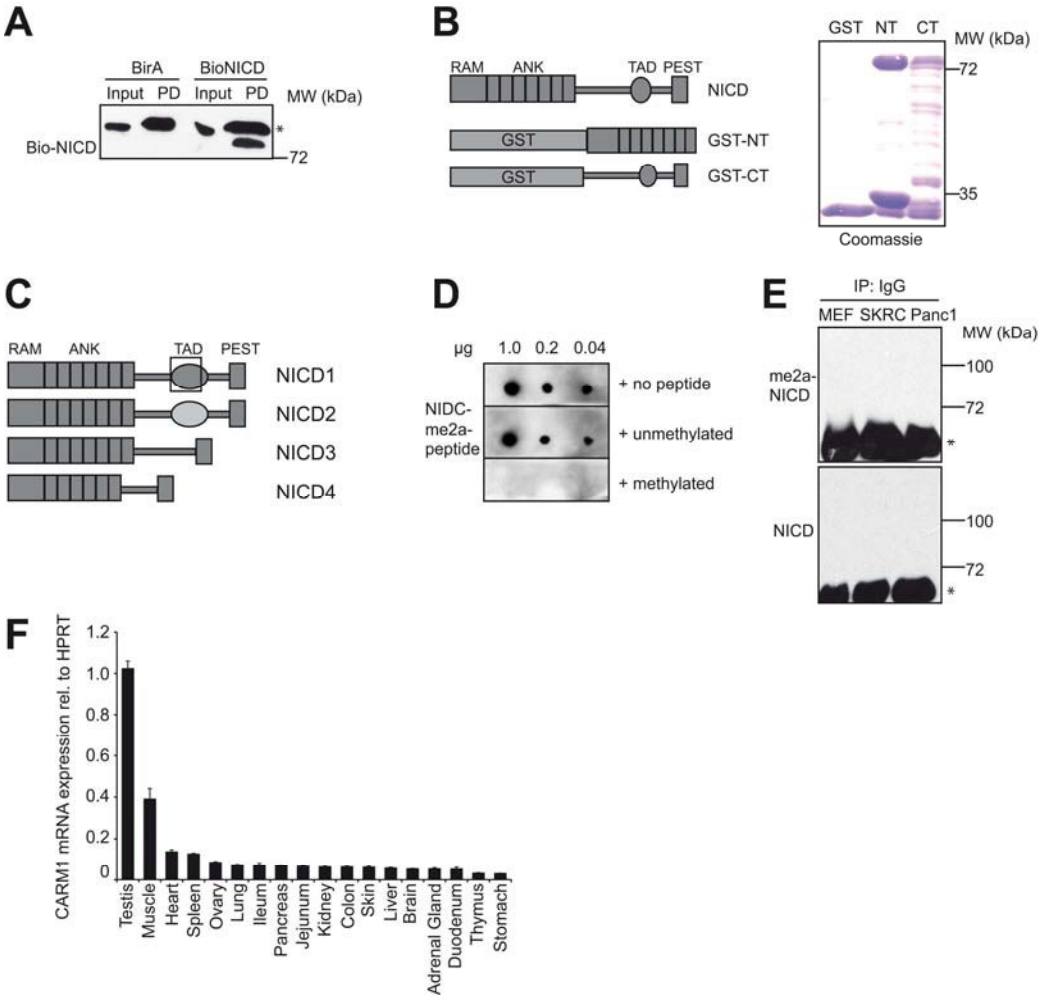

Fig. S1: Arginine residues in NICD are asymmetrically dimethylated and *CARM1* mRNA is expressed in adult mouse tissues. (A) Input control for biotinylated NICD (BioNICD) purified from Beko cells (Fig. 1A). **(B)** Schematic representation of the NICD constructs used for in vitro methylation assays. NICD was split in an N-terminal (NT) and a C-terminal (CT) fragment. Purification was confirmed by Coomassie staining. **(C)** Schematic domain structure of the four different Notch intracellular domains (NICD1-4) with the region containing the modified arginine residues indicated by the black rectangle. **(D)** In peptide competition assay recognition of the Arg^{2361}me2a peptide in dot blot is abolished after addition of the methylated peptide (10 ng/ml) to the antibody solution; the unmodified peptide did not have any effect. **(E)** Negative control (IgG) for pulldown of me2a-NICD in MEFs, SKRC cells, and Panc1 cells (see Fig. 2F). Blots are representative of 2 experiments. **(F)** Expression of *CARM1* in adult mouse tissues, normalized to that of endogenous *HPRT* mRNA in each. Data are means ± SD from four experiments. Blots are representative of 3 experiments.

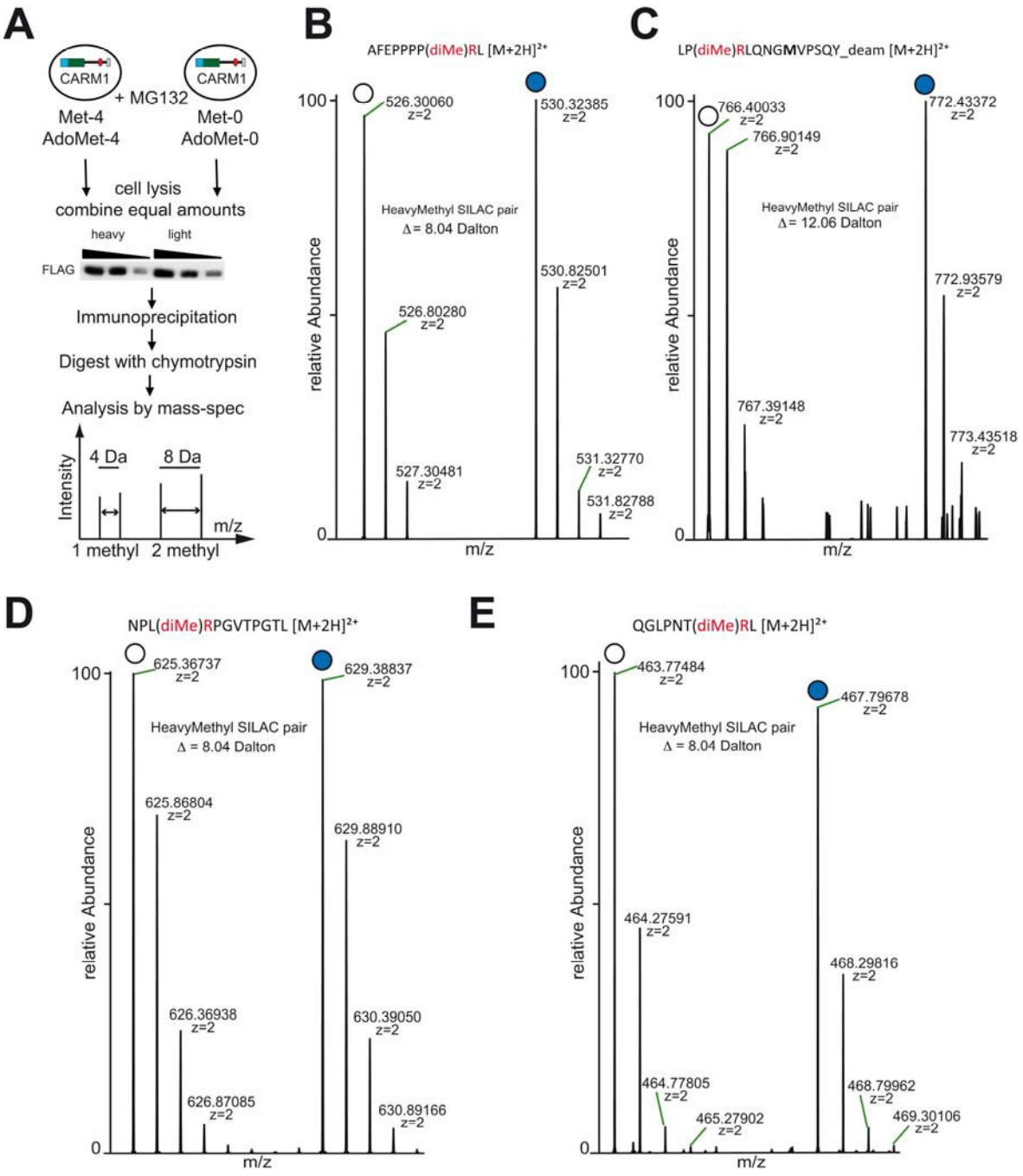

Fig. S2: Methylation sites identified by heavy methyl SILAC. (A) Setup of the Heavy-Methyl SILAC approach. 293 cells grown in heavy or light medium (different isotopes of methionine that get incorporated in the methylgroup donor adenosyl methionine, AdoMet) were transiently transfected with FLAG-NICD together with a construct expressing CARM1. After 6 hours of proteasome inhibitor treatment (MG132, 20 μM) the cells were lysed, equal input for heavy and light sample was determined and then mixed in a ratio of 1:1. After immunoprecipitation the sample was run on a SDS-PAGE gel. The NICD corresponding band was cut out, digested with chymotrypsin and further analyzed by mass spectrometry. Methylated samples show a specific difference of 4 Da per methyl group adapted from **(*26*).**

(B-E) Heavy-Methyl SILAC pairs of Arg^{2262} **(B)**, Arg^{2317} **(D)** and Arg^{2361} **(E)** are displayed that possess the specific difference of 8 Da for two methyl groups. For the dimethylated Arg^{2303} (**C**) the difference is 12 Da due to the presence of a methionine in the peptide. The white circle marks the unlabeled, blue the Heavy-Methyl SILAC-labeled spectrum. Data are representative of two experiments.

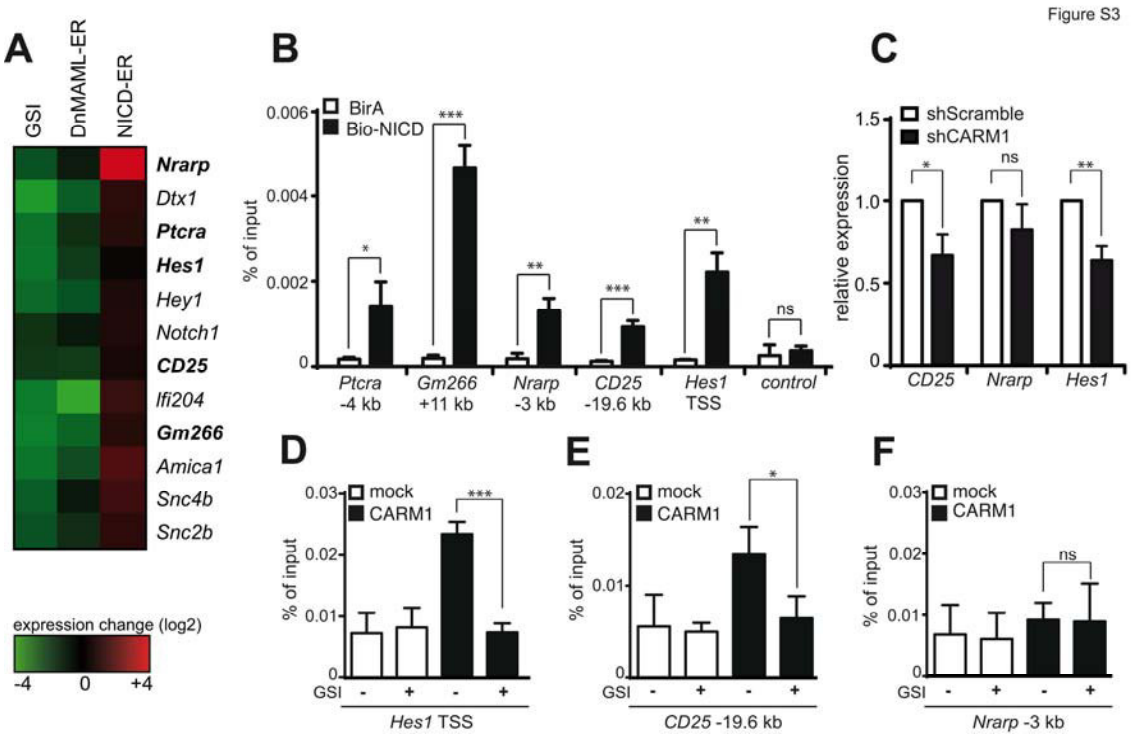

Fig. S3: Selection of direct Notch target genes in pre–T cells. (A) A selection of Notch target gene expression changes identified by microarray analysis (*55*) in Beko cells treated with the γ-secretase inhibitor (GSI) DAPT or induced by tamoxifen to induce dominant-negative Mastermind1 (DnMAML1)-ER or NICD-ER to translocate to the nucleus. **(B)** Binding of NICD to enhancers of Notch target genes in a stable pMY-Bio-NICD-IRES-GFP infected Beko cell line was detected by Streptavidin-ChIP. As control, BirA (biotin ligase)-transfected cells were used. Control locus: chromosome X. **P* = 0.0209, ***P* = 0.0035 (*Nrarp*) or 0.0014 (*Hes1*), ****P* = 0.0001 (*Gm266*) or 0.0008 (*CD25*). **(C)** Knockdown of CARM1 reduced the expression of Notch target genes *CD25* and *Hes1* in Beko cells. *P = 0.0111, ***P* = 0.0022, ns *P* = 0.1211. **(D-F)** Abundance of CARM1 on Notch1/RBP-J binding sites of *Hes1* (D), *CD25* (E) and *Nrarp* (F) detected by ChIP in Beko cells transfected with CARM1 or Protein A beads (mock). **P* = 0.0347, ****P* = 0.004, ns *P* = 0.9424. Data are means ± SD from three experiments. *P* values were calculated using the unpaired *t*-test.

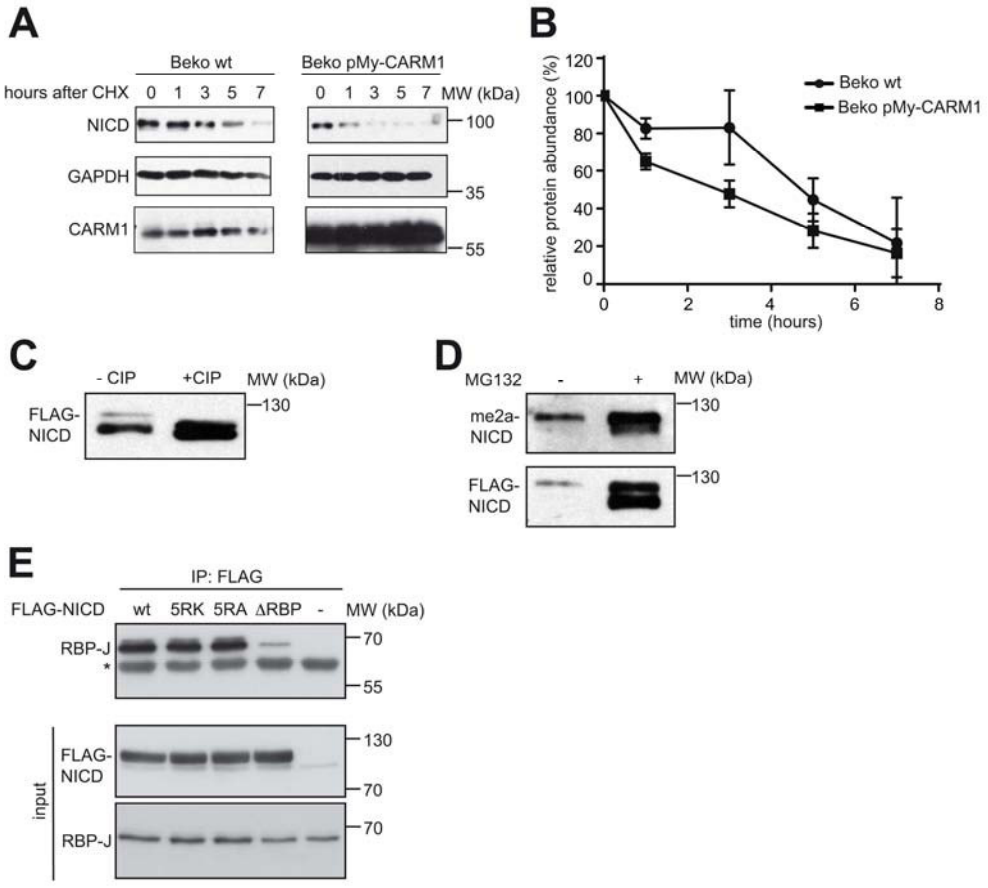

Fig. S4: Methylation of the NICD in the context of its stability, phosphorylation, and binding to RBP-J. (A and B) Western blotting shows the degradation of endogenous NICD in wild-type (wt) Beko cells or cells transfected with the CARM1 expression plasmid (pMY-CARM1), both treated with protein synthesis inhibitor cycloheximide (CHX, 50 µg/ml) for the indicated time. Relative NICD abundance was quantified by ImageJ software (B). Data are means ± SD from three experiments. **(C)** Cell extracts of 293 cells transfected with FLAG-NICD and treated with alkaline phosphatase (CIP). Upon treatment, the two bands were not distinguishable by Western blot. **(D)** Pulldown for total or methylated NICD in 293 cells transfected with wild-type FLAG-NICD and pMY-CARM1 and treated with either DMSO or MG132 for 6 hours. **(E)** Pulldown for RBP-J with FLAG-NICD in HEK 293 cells transfected with the indicated wild-type (wt) or mutant NICD construct. NICD-ΔRBP: 1758 WFP/LAA 1760 mutation in the RAM23 domain. The asterisk denotes the heavy chain of the antibody used for immunoprecipitation.

Arginine Residue	Mutation	Tissue	Nr	PMID and Reference	COSMIC Mutation ID
R2263	G2262fs*6	Haematopoetic and lymphoid tissue (T-ALL)	1	16707600 [66]	COSM21910
	S2163_S2283 del121	Haematopoetic and lymphoid tissue (CLL)	1	22077063 [67]	COSM255088
R2272	P2271S	Hematopoietic and lymphoid tissue (T-ALL), upper aerodigestive tract	1 1	21798897 [68] 16707600 [66]	COSM99629 COSM21911
	R2272fs*78	Hematopoietic and lymphoid tissue (T-ALL)	1	19458356 [69]	COSM36046
R2313	R2313G	Lung	1	22980975 [70]	COSM377778; COSM377779
R2327	R2327W	Large intestine, ovary, lung	2 1 1	21720365 [71] 20007775 [72]	COSM120008 COSM43356
	N2324fs*9	Haematopoietic and lymphoid tissue (T-ALL)	1	23354995 [73]	COSM1235034
R2372	S2329fs*25	Haematopoietic and lymphoid tissue (T-ALL, CLL)	3	19458356 [69]	COSM36047
	L2335fs*19	Haematopoietic and lymphoid tissue (T-ALL, CLL)	2	22077063 [67] 16614245 [74]	COSM28653

Table S1: Mutations at the methylated arginine or surrounding residues in Notch1. Mutations reported to occur at or near the methylated arginine residues in Notch1. Data was obtained from the COSMIC (Catalogue of Somatic Mutations in Cancer) database, http://cancer.sanger.ac.uk/cancergenome/projects/cosmic/ . Nr, number of samples with the corresponding mutation.

Construct	Primer	Sequence
pMY-Bio-CARM1	BglII fw NotI rev	agatctgcagcggcggcagcga gcggccgcctaactcccatagtgcatggtgtt
pcDNA3.1-CARM1-mut	EcoRI-fw NotI-rev	gaattcgcagcggcggcagcga gcggccgcctaactcccatagtgcatggtgtt
pCSGS-NICD-wt/5RA	SmaI fw SmaI rev	gccccgggcggcagcatggccagctctggtt gccccgggttatttaaatgcctctggaatgtgg
pGEX6P1-NICD-NT	EcoRI fw XhoI rev	gaattccggcggcagcatggccagc ctcgagtcacagctgtgggctgcgcacc
pGEX6P1-NICD-CT	EcoRI fw NotI rev	gaattcatcgtgcggcttttggat gcggccgctcatttaaatgcctctggaatgtg
pGE-basic	EGFP_NcoI_fw EGFP_XbaI_rev	atccatggtgagcaagggcg attctagattacttgtacagctcgtccatgc
pMIGR-mNICD-ER (wt or 5RK)	SalI fw SalI rev	gtcgacatggactacaaagacgatgac gtcgacgctttaaatgcctctggaatg

Table S2: Cloning primers used in this study. Fw, forward primer; Rev, reverse primer; sequences 5'-3'.

Position relative to TSS	Probe (Roche library)	ChIP primer sequence
MyoD TSS	#25	Fw: gtcagctccgaagtgagca Rev: cacttggctatctggtgcag
Ptcra -4 kb	#60	Fw: ctgcactgtggtcgcaga Rev: ggaggcaggtgtccctaac
Gm266 +11 kb	#17	Fw: cccaggtgactaagggacac Rev: gagactgactgttcccacgag
Hes1 TSS	#81	Fw: gccagaccttgtgcctagc Rev: tctttcccacagtaactttcagc
CD25 -19.6 kb	#21	Fw: ggctgttggagaccacga Rev: tcaattccaagaccttctttcc
Nrarp -3 kb	#66	Fw: cctatcctctcttctaccaggtgt Rev: tgggaaagaggagagtgtttct
Chrom. X	#68	Fw: gagttccagggactgtcacg Rev: atggtgtctacttgtaagcccagt

Table S3: ChIP primers used in this study. Fw, forward primer; Rev, reverse primer; sequences 5'-3'.

Gene	Probe (Roche library)	cDNA primer sequence
mus musculus		
HPRT	#25	Fw: tgtgggcattgtgctacct Rev: atttttgtcccggcgaac
Ptcra	#45	Fw: cagctctccttgccttctga Rev: cctggctgtcgaagattcc
Gm266	#81	Fw: caaggccgacctagatgc Rev: gtcgtgatttcaggaacg
Carm1	#26	Fw: tgtgggcagacagtccttc Rev: ccgacaggttttcaggatgt
Hes1	#99	Fw: acaccggacaaaccaaagac Rev: cgcctcttctccatgatagg
Nrarp	#49	Fw: gctacacatcgccgcttt Rev: ttggccttggtgatgagata
CD25	#89	Fw: caatggagtataaggtagcagtgg Rev: catctgtgttgccaggtgag
GusB	#25	Fw: tgtgggcattgtgctacct Rev: atttttgtcccggcgaac
Xenopus laevis		
hes5.1		Fw: ggaaaagatgcgcagagacag Rev: gggttcctgcttgtgaaattct
hes3.3		Fw: agatgcgcagggaccgtat Rev: ggctggaggagctggaattc
hes5.2		Fw: caaaagcagccagaaaccga Rev: atgatgaaatgcagctggca
hes9.1		Fw: atcgagcagctcaggatgtt Rev: tggtttggatgggagatgat
esr10		Fw: agcagcacatgacaaccaaa Rev: tgcagagagtcctggagaca
hey1		Fw: tgcaggaggcaaaggctact Rev: tgaatcccaagctgcggta
hes4		Fw: taccgacggccagtttgc Rev: atacagagggataacaggtccgg
dll1		Fw: gcagtaatgcggaccccac Rev: ccaggccatgtgaatccaa
tubb2b		Fw: agcagcacatgacaaccaaa Rev: tgcagagagtcctggagaca
hist1h4a		Fw: ggcaaaggaggaaaaggactg Rev: ggtgatgccctggatgttat

Table S4: qPCR primers used in this study. Fw, forward primer; Rev, reverse primer; sequences 5'-3'.

	BTD	RBP	RAM-ANK-RBP
RAM	31 nM, 72 nM[59,60]	22 nM[57, 58], 1100 nM[59,60*]	
RAM-ANK	200 nM[59,60]	14 nM[57, 58], 510 nM[59, 60*]	
DNA		200 - 300 nM[57, 58]	200-300 nM[57, 58]

Table S5: Available dissociation constants between the domains of NICD and RBP found in the literature. Dissociation constants reported in the literature by Blacklow and colleagues (56), Kovall and colleagues (57, 58), and Barrick and colleagues (59, 60). *, measured by FRET.